



HAL
open science

Dual control of Kinesin-1 recruitment to microtubules by Ensconsin in *Drosophila* neuroblasts and oocytes

Mathieu Métivier, Brigette Monroy, Emmanuel Gallaud, Renaud Caous, Aude Pascal, Laurent Richard-Parpaillon, Antoine Guichet, Kassandra Ori-Mckenney, Régis Giet

► To cite this version:

Mathieu Métivier, Brigette Monroy, Emmanuel Gallaud, Renaud Caous, Aude Pascal, et al.. Dual control of Kinesin-1 recruitment to microtubules by Ensconsin in *Drosophila* neuroblasts and oocytes. *Development* (Cambridge, England), 2019, 146 (8), pp.dev171579. 10.1242/dev.171579 . hal-02110975

HAL Id: hal-02110975

<https://hal.science/hal-02110975>

Submitted on 18 Jul 2019

HAL is a multi-disciplinary open access archive for the deposit and dissemination of scientific research documents, whether they are published or not. The documents may come from teaching and research institutions in France or abroad, or from public or private research centers.

L'archive ouverte pluridisciplinaire **HAL**, est destinée au dépôt et à la diffusion de documents scientifiques de niveau recherche, publiés ou non, émanant des établissements d'enseignement et de recherche français ou étrangers, des laboratoires publics ou privés.

Dual control of Kinesin-1 recruitment to microtubules by Ensconsin in *Drosophila* neuroblasts and oocytes.

Mathieu Métivier¹, Brigette Y. Monroy³, Emmanuel Gallaud¹, Renaud Caous¹, Aude Pascal¹, Laurent Richard-Parpaillon¹, Antoine Guichet², Cassandra M. Ori-McKenney³ and Régis Giet^{1*}.

¹. Univ Rennes, CNRS, IGDR (Institut de Génétique et Développement de Rennes) - UMR 6290, F-35000 Rennes, France

². Institut Jacques Monod-Université Paris Diderot-Paris 7, 15 rue Hélène Brion, 75205 Paris Cedex 13, France

³. University of California, Davis, One Shields Avenue, Davis, CA 95616, USA

* Corresponding author: regis.giet@univ-rennes1.fr

Abstract

Drosophila Ensconsin/MAP7 controls spindle length, centrosome separation in brain Neuroblasts (NBs) and asymmetric transport in oocytes. The control of spindle length by Ensconsin is Kinesin-1 independent but centrosome separation and oocyte transport requires targeting of Kinesin-1 to microtubules by Ensconsin. However, the molecular mechanism used for this targeting remains unclear. Ensconsin/MAP7 contains a microtubule-binding domain (MBD) and a Kinesin-binding domain (KBD). Rescue experiments show that only full length Ensconsin restores the spindle length phenotype. KBD expression rescues *ensc* centrosome separation defects in NBs, but not the fast oocyte streaming and the localization of Stauf and Gurken. Interestingly, the KBD can stimulate Kinesin-1 targeting to MTs *in vivo* and *in vitro*. We propose that the KBD/Kinesin-1 is a minimal activation module that increases Kinesin-1 affinity for MTs. Addition of the MBD present in full length Ensconsin allows this process to occur directly on the microtubule and triggers higher Kinesin-1 targeting. This dual regulation by Ensconsin is essential for optimal Kinesin-1 in oocytes, but not in NBs, illustrating the importance of adapting Kinesin-1 recruitment to different biological contexts.

Introduction.

Microtubules (MTs) are dynamic polymers that grow and shrink over time, a process known as dynamic instability (Mitchison and Kirschner, 1984). They are regulated by microtubule-associated proteins (MAPs), which have a wide range of activities. MAPs can modify microtubule dynamic parameters, and are able to organize microtubules into complex structures. The MAP family also includes microtubule motors that slide along the MTs. These motor proteins use ATP hydrolysis to move cargo along microtubules, thus transporting vesicles, chromosomes, proteins, RNA, and even other microtubules. MT networks and their associated MAPs therefore play key roles in various biological processes, including cell division, intracellular trafficking, and cell morphogenesis (Barlan and Gelfand, 2017; Heald and Khodjakov, 2015; Walczak and Heald, 2008).

Enscinsin/MAP7 was first identified in microtubule preparations isolated from epithelial cells (Bulinski and Bossler, 1994). The protein has been given several names, including epithelial MAP of 115 kD (E-MAP115) and Ensconsin, due to its tenacious association with microtubules both *in vivo* and *in vitro* (Bulinski and Bossler, 1994). Ensconsin/MAP7 is associated with the interphase microtubule cytoskeleton, but its overexpression in cultured cells does not seem to affect microtubule dynamics during interphase, and instead mitotic abnormalities frequently occur during cell division (Faire et al., 1999).

The possible function of Ensconsin remained elusive for a decade, until *ensc* mutant flies were isolated in a screen for genes affecting *Drosophila* female germ line development. *ensc* mutant females are sterile, and oocytes display microtubule-dependent mislocalization of several polarized key molecules required for the proper patterning of developing embryos. These molecules include *oskar* mRNA and its binding partner, the Staufén adaptor protein, on the posterior side (Ferrandon et al., 1994; St Johnston et al., 1991; Sung et al., 2008), and the Gurken protein, a TGF beta like ligand on the dorso-ventral axis (Neuman-Silberberg and Schupbach, 1993; Sung et al., 2008). The *ensc* mutant oocytes also show absent microtubule-dependent streaming of granules (Sung et al., 2008). Interestingly, these defects are shared by Kinesin heavy chain (KHC) mutants (Brendza et al., 2000; Brendza et al., 2002; Duncan and Warrior, 2002; Januschke et al., 2002). In *ensc* oocyte extracts, the recruitment of Kinesin-1 motors to MTs is impaired *in vitro*, and it has recently been shown that purified Ensconsin/MAP7 proteins can directly recruit Kinesin-1 to the MT *in vitro*, providing evidence for a model in which Ensconsin/MAP7 stimulates recruitment of Kinesin-1 to MTs (Sung et al., 2008). This recruitment model is also evident in mouse and *Drosophila* muscle

cells. In these large cells, both Ensconsin and Kinesin-1 are required to promote nuclei positioning and spacing, processes required for correct muscle function. In this study, the authors also showed a direct physical association between the Kinesin-1 motor and the Ensconsin C-terminal domain (the Kinesin-binding domain, or KBD). Furthermore, after Kinesin-1 or Ensconsin knock down, a fusion between the Ensconsin N-terminal MT-binding domain (MBD) and the Kinesin-1 motor domain is sufficient to rescue nucleus-positioning defects (Metzger et al., 2012). Together, the studies of muscle cells and fly oocytes cited here support a model in which Ensconsin favours Kinesin-1 microtubule recruitment via its MBD and KBD domains (Metzger et al., 2012; Sung et al., 2008). However, a second model, based on S2 cultured cell studies, proposes that some Ensconsin function does not depend on the MBD. For these functions, Kinesin-1 can be recruited solely by the KBD (Barlan et al., 2013), showing that microtubule targeting by Ensconsin is not an absolute requirement for Kinesin-1 function.

Here, we used a combination of genetic studies with rescue constructs at different stages of fly development as well as *in vitro* experiments to unambiguously show that Kinesin-1 is actually subjected to a dual recruitment mode by Ensconsin that synergizes its loading onto microtubules.

Materials and Methods.

DNA constructs

Histidine-tagged expression constructs were generated as previously described using full-length Enscinsin; Ensc-MBD, the N-terminal domain which contains the microtubule-binding domain, also referred to as EHR1; and Ensc-KBD, the C-terminal domain containing the Kinesin-binding domain, also referred to as EHR2 (Gallaud et al., 2014; Sung et al., 2008). Ensc-MBD and Ensc-KBD were also introduced into the pUWG vector to generate fly expression constructs for the ubiquitous expression of GFP-tagged proteins. Full-length Enscinsin was introduced in pTWV vector to generate over expression of a VenusFP-protein under the control of the GAL protein. pUWG and pTWG were purchased from the Drosophila Genomics Resource Center (Indiana University). The *Drosophila* Kinesin-1 expression construct K560 (amino acid 1-560, gift from R. Vale) was cloned in frame using Gibson cloning into pET28 vector with a C-terminal mScarlet-strepII cassette (Monroy et al., 2018).

Fly strains

Flies were maintained under standard conditions at 25°C. All studies were performed using *ensc Δ null* and *ensc Δ N ensconsin* mutants (Sung et al., 2008). In contrast with previous studies, Western blotting experiments using an antibody raised against the C-terminal region of Enscinsin revealed the *ensc Δ N allele* is a null allele (Gallaud et al., 2014). *ensc Δ null* is also a null allele but the deletion also removes a piece of the neighbouring gene (Sung et al., 2008). All experiments were therefore performed in trans-heterozygous *ensc Δ null/ensc Δ N* flies, hereafter referred to as *ensc* flies. *khc* mutant flies carrying amino-acid substitutions have been described elsewhere and were provided by A. Guichet (Institut Jacques Monod, Paris, France), B. Saxton (University of California, Santa Cruz, Santa Cruz, CA), and A. Ephrussi (European Molecular Biology Laboratory, Heidelberg, Germany) (Djagaeva et al., 2012). We showed in a previous study that the combination of *khc²⁷* (null allele) and *khc⁶³* (hypomorphic allele) used in this study exhibited severe centrosome separation defects before mitosis (Gallaud et al., 2014).

Transgenic flies were obtained from BestGene (Chino Hills, CA) following P-element-mediated transformation with the pTWV vector containing full-length Enscinsin, or the pUWG vector containing the FL-Ensc, Ensc-KBD, or Ensc-MBD sequences. The Ensc-GFP and the Ensc-KBD-GFP but not the Ensc-MBD-GFP transgenic proteins rescued the semi-

lethality of the *ensc* Δ *null* and *ensc* Δ *N* mutants and the trans-heterozygous *ensc* flies. Unless specified, Ensc-GFP, KBD-GFP and MBD-GFP refer to transgenic animals expressing the corresponding GFP-tagged proteins in an *ensc* background.. RFP-tubulin expressing flies were given to us by Renata Basto (Institut Curie, Paris). The 69B-GAL4 strain is from Bloomington Stock Center and was used to drive over expression of Enscinsin-Venus in brain tissues (Ensc OE). All other GFP and RFP fusion proteins were ubiquitously produced under the control of the polyubiquitin promoter.

Antibodies and western blotting

The monoclonal YL1/2 rat anti-detyrosinated tubulin antibody (1:200) and the mouse monoclonal and rabbit polyclonal anti-phosphorylated histone H3 (Ser10) antibodies (1:500) were obtained from Millipore. The mouse anti-GFP monoclonal antibody (1:1000) was obtained from Roche. The rabbit and rabbit anti-actin (1:4000) polyclonal antibodies, the anti-Staufen antibody (1:1000) came from Santa Cruz Biotechnology. The rabbit polyclonal anti-KHC antibody (1:2000) was obtained from Cytoskeleton. The mouse monoclonal anti-Gurken antibody (1:200) was from the Developmental Studies Hybridoma Bank. The making of the anti-Enscinsin antibody was previously described, and the antibody was raised against the Kinesin-binding domain (Gallaud et al., 2014). The goat peroxidase-conjugated secondary antibodies (1:5000) were obtained from Jackson ImmunoResearch, and donkey Alexa fluor-conjugated secondary antibodies (1:1000) came from Life Technologies. For western blotting, ECL reagent was purchased from Thermo Fisher Scientific.

Live microscopy

Brains expressing the various GFP- or RFP-tagged proteins were dissected in Schneider's *Drosophila* medium containing 10% FCS. Isolated brains were loaded and mounted on stainless steel slides. The preparations were sealed with mineral oil (Sigma) as previously described (Gallaud et al., 2014). Images were acquired using a spinning-disk system mounted on an Eclipse Ti inverted microscope (Nikon) equipped with a 60X 1.4 NA objective at 25°C. Z-series were acquired every 30 or 60 seconds with a Photometrics CCD camera (CoolSNAP HQ2) and an sCMOS ORCA-Flash4.0 (Hamamatsu) controlled by MetaMorph acquisition software (version X). Images were processed using ImageJ software and are presented as maximum-intensity projections. Embryos were collected on agar plates supplemented with grape juice at 25°C. They were dechorionated by hand using double-sided adhesive tape, then mounted in mineral oil as previously described (Giet et al., 2002). Z-series images were

acquired every 30 seconds using either a spinning disk system or a Leica SP5 confocal microscope equipped with a 40X 1.3NA objective at 25°C. For ooplasmic streaming analyses, young females were mated with males and fattened with dried yeast for 3 (Controls, KBD-GFP or *Ensc-GFP*) to 5 days (MBD-GFP or *ensc*), anesthetized and their ovaries were removed from the abdomen with fine forceps. Stage 10B oocytes were isolated with two 27-gauge syringes needles in Halocarbon oil (Sigma), mounted and observed by light microscopy using a DMRXA2 microscope (Leica). Velocity analyses of the particles were performed as described in two separate studies ((Lu et al., 2016; Serbus et al., 2005)) except that three kymographs were obtained for each oocyte along active flows and 5 particles (15 per oocyte) were analysed for each kymograph using the Multikymograph plugin for Fiji.

Observation of *Ensc-GFP*, *KBD-GFP*, and *MBD-GFP* was performed in young oocytes also expressing RFP-tubulin after fast dissection of the ovary in PBS and direct observation of the live tissues under the microscope.

The analysis of centrosome separation in larval brain neuroblasts was performed as described before (Gallaud et al, 2014). The mother and daughter centrosomes were easily distinguished by their different microtubule nucleation potentials shortly before mitosis (Rebollo et al., 2007). Briefly, the separation angle between the 2 centrosomes was determined 30 sec before NEBD, by drawing a line crossing the mother centrosome, the nucleus centre and the daughter centrosome and calculated using the angle measurement tool for Fiji. In control neuroblasts, most centrosomes are fully separated before mitosis and this angle is between 120 and 180°.

Immunofluorescence in fly oocytes

Oocytes were collected from two-day-old females. To visualize the MT network, Endogenous *Ensc*, *KHC*, and *Ensc-GFP* fusion protein, oocytes were permeabilized at 25°C in 1% Triton X100 in BRB80 buffer (80 mM K-PIPES, 1 mM MgCl₂, 1 mM EGTA, pH 6.8) and fixed with cold methanol as described (Januschke et al., 2006).

For *Staufen* and *Gurken* localization, 4-8 ovaries were fixed with PBS buffer containing 4% paraformaldehyde and 0.1% Triton X-100, washed 3 times 5 min in PBST (PBS + 0.1% Triton X-100) and blocked on PBST containing 1% BSA. Incubation with the primary antibodies was performed overnight at room temperature in BBT (PBS containing 0.1% BSA and 0.1% Tween 20). The ovaries were then briefly washed 3 times and 3 times for 30 min each in BBT. The Alexa-conjugated secondary antibody was incubated for 2 h at room temperature. The ovaries were then washed 3 times for 15 min each time in PBST, dissected, and mounted in ProLong Gold (Invitrogen).

Immunofluorescence in fly brain by methanol fixation.

WT or *khc*²⁷/*khc*⁶³ larval brains were dissected in Schneider media supplemented with 10% of decompemented Foetal Calf serum (Invitrogen). When five brains were dissected, they were transferred in 20 µl of Schneider media. The brains were then gently aspirated with the tip of a Pasteur pipette and immediately transferred in 1 ml of methanol pre-chilled at -20°C. The tubes were then transferred for 15 min at -20°C. After fixation, the methanol was discarded and the tissues were washed 3 times 5 min in PBST with gentle agitation at room temperature, blocked with PBSTB (PBST supplemented with 1% BSA), and incubated with primary antibodies overnight at 4°C in PBSTB. The brains were then washed 3 times for 15 min in PBST and incubated with secondary antibodies for two hours at room temperature in PBSTB. After 3 washes in PBST, the tissues were mounted in ProLong Gold (Invitrogen).

Protein Expression and Purification

Tubulin was isolated from porcine brain using the high-molarity PIPES procedure as previously described (Castoldi and Popov, 2003). For bacterial expression K560-mScarlet, BL21-RIPL cells were grown at 37°C until ~O.D. 0.6 and protein expression was induced with 0.1 mM IPTG. Cells were grown overnight at 18°C, harvested, and frozen. Cell pellets were resuspended in lysis buffer (50 mM Tris pH 8, 150 mM K-acetate, 2 mM Mg-acetate, 1 mM EGTA, 10% glycerol) with protease inhibitor cocktail (Roche), 1 mM DTT, 1 mM PMSF, and DNaseI. Cells were then passed through an Emulsiflex press and cleared by centrifugation at 23,000 x g for 20 mins. Clarified lysate was passed over a column with Streptactin Superflow resin (Qiagen). After incubation, the column was washed with four column volumes of lysis buffer, then bound proteins were eluted with 3 mM desthiobiotin (Sigma) in lysis buffer. Eluted proteins were concentrated on Amicon concentrators and passed through a superose-6 (GE Healthcare) gel-filtration column in lysis buffer using a Bio-Rad NGC system. Peak fractions were collected, concentrated, and flash frozen in LN₂. Protein concentration was determined by measuring the absorbance of the fluorescent protein tag and calculated using the molar extinction coefficient of the tag. The resulting preparations were analyzed analysed by SDS-PAGE. Bacterial expression of hexa histidine-tagged KBD was performed as described before (Gallaud et al., 2014) except that the protein was dialysed overnight against PBS, and concentrated using Amicon Ultra-4 Centrifugal filters (Millipore). The proteins were stored at -80°C.

Immunoprecipitation experiments.

30 females expressing either MBD, KBD or full length GFP-tagged Ensconsin were lysed using a French press in 500 μ l of lysis buffer (LB 10 mM Tris, 150 mM NaCl, 0.5 mM EDTA, pH 7.4) supplemented with 0.05% NP-40, 1 mM DTT containing 5X proteases inhibitors (Roche). The extracts were centrifugated 10,000 g for 30 min at 4°C and the supernatants were incubated with 10 μ l of GFP-Trap beads (Chromotek) for 1 hour on a rotating wheel. The beads were washed 3 times with LB and the bound proteins were analysed by Western blotting using anti-GFP and anti-KHC antibodies.

Microtubule Co-sedimentation Assay

Microtubules were prepared by polymerizing 25 mg/mL of porcine tubulin in assembly buffer (BRB80 buffer supplemented with 1mM GTP, 1mM DTT) at 37°C for 15 min, then a final concentration of 20 μ M taxol was added to the solution, which was incubated at 37°C for an additional 15 min. Microtubules were pelleted over a 25 % sucrose cushion at 100,000g at 25°C for 10 min, then resuspended in BRB80 buffer with 1mM DTT and 10 μ M taxol. Binding reactions were performed by mixing 500 nM of sfGFP-Ensconsin-KBD and/or 500 nM mScarlet-K560 (that had been pre-centrifuged at 100,000g) with 2.5 μ M of microtubules in assay buffer (50 mM Tris pH 8, 50 mM K-acetate, 2 mM Mg-acetate, 1 mM EGTA, 10% glycerol and supplemented with 1 mM DTT, 10 μ M taxol) and incubated at 25°C for 10 min. The mixtures were then pelleted at 90,000g at 25°C for 10 min. Supernatant and pellet fractions were recovered, resuspended in sample buffer, run on an SDS-PAGE gel, then stained with Coomassie blue. Protein band intensities were quantified using ImageJ.

Statistical Analysis

All statistical tests were performed with Wilcoxon test or with two-tailed Student's t-test for MT co-pelleting assays.

Results.

***In vivo* functional analysis of the different domains of Ensconsin**

A previous study identified two Ensconsin deletion mutants named *ensc* Δ *Null* and *ensc* Δ *N*, expressing respectively no protein or leaving the C-terminal Kinesin Binding Domain intact (Sung et al., 2008). However, Western blotting analyses showed that these two mutants do not express detectable Ensconsin protein or truncated products and are therefore null alleles (see Material and Methods for details, and (Gallaud et al., 2014). To investigate the roles of the Ensconsin functional domains (microtubule-binding and kinesin-binding), we generated several fly lines. These expressed full-length Ensc-GFP, Ensc-MBD-GFP, or Ensc-KBD-GFP, under the control of the poly ubiquitin promoter. These lines were then used for rescue experiments in *ensc* mutant flies (Figure 1A, and Materials and Methods). We used Western blots to monitor the expression of the GFP-tagged Ensconsin variants in brain extracts. The exogenous full-length Ensc-GFP appeared as a 150-kDa doublet in Western blots, and it was expressed at levels similar to those of endogenous Ensconsin (Figure 1B, middle panel, lanes 6-7). The MBD-GFP (Figure 1B, top panel, lanes 2-3), and KBD-GFP proteins (lane 5), appeared as 70 and 100-kDa bands, respectively, and were expressed at similar levels as Ensc-GFP (lane 7). In *ensc* mutant flies, Ensc-GFP expression rescued the partial lethality and restored female fertility. However, the expression of MBD-GFP as tested in three independent transgenic lines failed to do so. In contrast, in two independent lines, KBD-GFP expression in *ensc*-null mutant flies rescued the partial lethality as much as wild-type Ensc-GFP, which suggests that this domain is sufficient for fly development into adulthood. However, we noticed that the Ensc-KBD female flies remained sterile, suggesting that the KBD alone is not enough to fully restore some aspects of oocyte development. To show that Ensconsin was able to physically interact with Kinesin-1, we performed immunoprecipitation experiments using whole female fly extracts expressing the GFP tagged proteins (see Methods, and Figure 1 C, top panel). We found that both Ensc-GFP and KBD-GFP, but not MBD-GFP proteins were able to interact with KHC (Figure 1 C, bottom panel) similarly to vertebrate Ensconsin/MAP7 (Hooikaas, 2018; Metzger et al., 2012).

The Ensconsin KBD fully rescues Kinesin-dependent centrosome separation defects in fly neuroblasts.

A previous study has shown that Ensconsin stimulates microtubule growth during mitosis. Consequently, *ensc* mitotic spindles are 20% shorter than their WT counterparts in neural stem cells (neuroblasts, NBs) (Gallaud et al., 2014). In addition, overexpression of Ensconsin (Ensc OE) in brain neuroblasts triggers the formation of longer and bent mitotic spindles (Figure S1). The fly NB divides asymmetrically to generate a renewing NB and a smaller cell subjected to differentiation. In this cell type, centrosome separation is initiated after the mother centrosome loses its MT nucleation potential. As a consequence, it is inherited in the differentiating cell, while the new centrosome retains MT nucleation and stays in the renewing NB (Conduit and Raff, 2010; Gallaud et al., 2014; Januschke et al., 2011; Rebollo et al., 2007; Rusan and Peifer, 2007). Ensconsin and Kinesin-1 are both required during interphase to promote centrosome separation in NBs. In *ensc* and *khc²⁷/khc⁶³* hypomorphic mutants, the centrosome separation does not occur after cytokinesis, but instead just before mitosis, leading to frequent mis-segregation of mother and daughter centrosomes (Gallaud et al., 2014). To challenge for a possible cooperation between Ensconsin and Kinesin-1, we analyzed centrosome separation in *khc²⁷/khc⁶³* hypomorphic NBs after Ensconsin overexpression (Ensc OE). We found Ensc OE completely rescued the centrosome separation defects in *khc* mutant neuroblasts, indicating that Ensc OE was able to boost the low Kinesin-1 activity of this hypomorphic *khc²⁷/khc⁶³* mutant. By contrast, *khc* mutations did not trigger spindle shortening of the long and bent spindles obtained following Ensc OE, in agreement with the fact that the regulation of the NB spindle length is a Kinesin-1 independent process (Gallaud et al., 2014, Figure S1A-D and supplementary Video 1-4). Importantly, KHC protein levels were normal in *ensc* mutant, and vice versa indicating that the stability of one protein was independent upon the presence of the other (Figure S1F). In addition, Ensconsin-Venus and endogenous Ensconsin localization (Figure S1 G and E) were not affected in a *khc* background. This indicates that Ensconsin protein stability and Ensconsin localization is Kinesin-1 independent but that Ensconsin OE can stimulate low Kinesin-1 activity.

In parallel, we measured the angles between the two centrosomes shortly before the nuclear envelope breakdown (NEBD), as readout for centrosome separation. In agreement with cooperation between Kinesin-1 and Ensconsin during interphase, we found that elevating the levels of Ensconsin protein (Ensconsin Overexpression: Ensc OE) completely rescued the centrosome separation defects in *khc* mutant neuroblasts, indicating that Ensc OE was able to boost the low Kinesin-1 activity of *khc²⁷/Khc⁶³* mutant. By contrast, *khc* mutations did not

trigger spindle shortening of the long and bent spindles obtained following *Ensc* OE, in agreement with previous observations indicating that spindle length is independent of Kinesin-1 activity (Gallaud et al., 2014, Figure S1A-D and supplementary Video 1-4).

We then monitored the ability of GFP-tagged *Ensc* variants to rescue spindle length and centrosome separation defects observed in *ensc* mutants. To do this, we used live microscopy on *Ensc*-GFP, KBD-GFP, and MBD-GFP variants co-expressing RFP-tubulin. In control NBs (Figure 2A, F-H, Supplementary Video 5), the centrosomes were fully separated before NEBD, as the angle between the two centrosomes and the nucleus centre was between 120 and 180° (100%, $n=30$). In *ensc* mutants (Figure 2B, F-H, Supplementary Video 6), most cells displayed incomplete centrosome separation before mitosis, as most of the angles between the two centrosomes and the nucleus center were between 60 and 120° (61.9%, $n=21$), but this defect was restored by *Ensc*-GFP expression, after which 100% ($n=19$) of the NBs showed pre-NEBD centrosome separation that was comparable to the control (Figure 2C, G-H Supplementary Video 9). *ensc* mutant NBs expressing MBD-GFP showed centrosome separation defects similar to those of the *ensc* mutants (58.8% between 60 and 120°, $n=17$, Figure 2D, F-H, Supplementary Video 7). In *ensc* mutant NBs expressing KBD-GFP, centrosome separation was restored (87% above 120°, $n=23$), suggesting that this domain can efficiently rescue the centrosome separation defects on its own (Figure 2E, F-H, Supplementary Video 8). Interestingly, this rescue of centrosome-separation defect did not require microtubule binding as the KBD was not detected on MTs in squashed preparations (Figure 2E, middle panels).

Efficient mitotic spindle assembly was assayed by spindle length measurements. *Ensc* variant rescue of mitotic spindle length associated with *Ensc* deletion indicated that only *Ensc*-GFP, and not *Ensc*-KBD or *Ensc*-MBD, was able to restore normal spindle size. This demonstrates that mitotic spindle length control in neuroblasts requires full-length *Ensc*, and that MBD-GFP and KBD-GFP are unable to restore correct spindle length individually (Figure 2I, and Supplementary Video 5-9).

The *Ensc* KBD is not sufficient for ooplasmic streaming and the correct targeting of Staufen and Gurken in the oocyte.

A previous study has shown that *Ensc* is required for Staufen and Gurken transport in the oocyte to the posterior and the antero-dorsal regions, respectively (Sung et al., 2008).

We first checked that the MBP-GFP, KBD-GFP and *Ensc*-GFP proteins were expressed in oocytes by live immunofluorescence analyses and Western Blotting of oocyte extracts (See Methods for details and Figure S4 A and B).

We then monitored the localization of Gurken in *ensc* mutant oocytes expressing *Ensc*-GFP, KBD-GFP, or MBD-GFP at stages 9 (Figure S2). In most WT (71%, $n=14$) and *Ensc*-GFP oocytes (72%, $n=18$), Gurken was tightly localized at the cortical antero-lateral corner (Figure S2 A top, C). By contrast, a majority of, *ensc* (70% $n=23$) and *Ensc*-MBD (81%, $n=15$) oocytes showed that the Gurken protein appeared as a punctiform pattern spread around the nuclear region (Figure S2 A bottom panels, B and C). KBD-GFP oocytes had an intermediate phenotype and half of these oocytes showed abnormal or incomplete Gurken localization (52%, $n=12/23$, Figure S2).

At the same time, we also monitored Staufen's localization at the posterior cell cortex (Figure 3). During oogenesis, two Kinesin-1-dependent pathways are used to transport Staufen particles to the posterior pole of the embryo, where Myosin V captures them. At stage 9, Staufen is transported directly by Kinesin-1 through the network of polarized microtubules whose plus end is directed towards the posterior cortex (Figure 3D, top left see also (Lu et al., 2018; Lu et al., 2016)). At stage 10B, Staufen particles are transported via ooplasmic streaming: a fast and important movement of particles on mobile microtubules that slide on a population of stable microtubules that are anchored to the cortex of the ovarian chamber (Lu et al., 2018; Lu et al., 2016).

At stage 9, we found that *Ensc*-GFP (Figure 3A e, $n=9$) was able to fully rescue Staufen's cortical posterior localization similarly to the controls (Figure 3A panel a, $n=13$). In contrast, both in *ensc* (Figure 3A panel c, $n=5$) mutant oocytes and in those where MBD-GFP was expressed (Figure 3A panel g, $n=8$), Staufen displayed a crescent intensity that was about five times weaker than that of WT (Figure 3 B). Expression of KBD in *ensc* mutant oocytes ($n=17$) allows Staufen to be targeted to the posterior pole in stage 9 oocytes, and the crescent intensities reached 74% of the control values although the protein appeared mislocalized in some case (Figure 3A panel panel i, red arrow, and Figure 3 B). At Stage 10B, *Ensc*-GFP ($n=13$) and WT ($n=15$) oocytes showed a normal Staufen crescent at the posterior pole (Figure 3 A, compare panel b and f) while the intensity was weak in *ensc* (Figure 3 A, panel

d, $n=11$) and MBD oocytes (Figure 3 A, panel h, $n=9$). KBD oocytes (Figure 3J, $n=14$) showed an intermediate phenotype and the Staufen crescent intensity was 50 % of the value observed in controls (Figure 3A panel j and Figure 3 C). Because Kinesin-1 dependent ooplasmic streaming participates in Staufen targeting to the posterior cortex in stage 10B oocytes, we monitored the ability of our different Ensconsin variants to restore this process (Palacios and St Johnston, 2002; Serbus et al., 2005; Sung et al., 2008) (Figure 3, E-F). We found, as described before that *ensc* oocytes ($n=15$) showed no ooplasmic streaming, as well as MBD-expressing oocytes ($n=13$, Figure 3F and G). However, expression of Ensconsin-GFP ($n=16$) efficiently restored ooplasmic particle velocity ($n=11$ oocytes, 123 nm/sec, Figure 3, F-G). KBD-GFP expressing oocytes showed a complete absence ($n=17/23$) or a very slow ($n=6/23$) ooplasmic streaming ($n=6/23$ oocytes, 10 nm/sec). To summarize, our data show that Ensconsin KBD is able to sustain efficient Staufen targeting during stage 9 of oogenesis but it fails to promote ooplasmic streaming and consequently the next step of Staufen polarization during stage 10B..

The Ensconsin KBD promotes minimal recruitment of Kinesin-1 on the oocyte MT network.

Kinesin-1 can bind to Ensconsin, and the correct targeting/loading of this motor on MTs is essential for Kinesin-1 function (Metzger et al., 2012). We confirmed as described before, that endogenous Ensconsin is located in the oocyte egg chamber during early stages of oogenesis and also co-localized with the MT cytoskeleton of stage 9 and 10B respectively (Figure S4C, (Sung et al., 2008)). We decided to examine the localization of Kinesin-1 in oocytes at stage 9 and 10B, the two developmental stages that requires Kinesin-1 for direct transport of Staufen particles to the posterior cortex, and for ooplasmic streaming respectively. The microtubule network of the egg chamber was challenging to detect because of the high background caused by the presence of free tubulin dimers. Thus, to visualize the microtubule network, as well as MT-associated Kinesin-1 inside the egg chamber, it was necessary to permeabilize the oocyte for one hour in a MT stabilizing buffer before methanol fixation (Januschke et al., 2006). In control stage 9 oocytes, KHC appeared to be located on the polarised MT network, but the majority of KHC was located at the posterior pole (Figure 4 A top). In *ensc* and MBD oocytes (Figure 4A, second and fourth panels from top), this localization pattern was completely impaired. Interestingly, KHC total protein levels were comparable to control extracts in *ensc* mutants, when analysed by Western blot, suggesting that the ability of KHC to bind MTs was impaired following loss of Ensconsin but not KHC

stability (Figure 4 A-C and S3A right panels). In addition and similarly to brain tissues, Ensconsin protein levels as well as its ability to bind oocyte MTs was Kinesin-1 independent (Figure S3A left panel, B). Expression of *Ensc*-GFP completely rescued the correct localization of KHC localization to the posterior pole and on the MT network (Figure 4A, third panels). Interestingly, at the corresponding stage 9, KHC was present on the MT network and 50 % of the pool of KHC appeared to be targeted to the posterior cortex in KBD-GFP oocytes (Figure 4 A bottom panels and Figure 4 B).

In WT stage 10B oocytes ($n=10$), Kinesin-1 heavy chain (KHC) was strongly bound to the internal oocyte MT network utilized for the process of oocyte streaming, similar to previous observations (Januschke et al., 2006) (Figure 4C, top panels). On the other hand, KHC localization was absent on the MT network of *ensc* oocytes ($n=7$, Figure 4, second panels from top). This localization was fully restored by the expression of *Ensc*-GFP ($n=15$, Figure 4, third panels from top), but not by MBD-GFP ($n=13$ Figure 4, fourth panels from top). In KBD-GFP-expressing oocytes ($n=9$), the MT network showed a very weak presence of Kinesin-1 (Figure 4, bottom panels). In most cases, KHC appeared to aggregate around the MT network of these KBD oocytes rather to be co-localized with MT bundles (purple arrows). Altogether, these results suggest that KBD is sufficient to fully rescue centrosome-separation defects in brain NBs (Figure 2) and to recruit of Kinesin-1 in stage 9 but not in stage 10B oocytes. Interestingly and similarly to previous observations, the cytoplasmic arrays of MT bundles in stage 10B oocytes was severely disrupted following *khc* RNAi (Figure S3B and (Lu et al., 2016; Serbus et al., 2005). This was also the case when KHC was not targeted to the MTs by Ensconsin in stage 10B oocytes (Figure 4 C, in *ensc*, MBD and KBD oocytes). To conclude, the presence of Kinesin-1 and also its MT targeting by Ensconsin is required to promote MT bundling and organisation and ultimately oocyte streaming during stage 10B of oogenesis.

The Ensconsin KBD recruits Kinesin-1 to MTs *in vitro*.

To assess whether the KBD recruits Kinesin-1 to MTs directly, we used an *in vitro* approach with purified components (Figure 5B). We performed a co-sedimentation assay with purified proteins and taxol-stabilized microtubules to analyse the effect of KBD on a truncated *Drosophila* Kinesin-1 protein (K560) recruitment in an excess of MTs (Monroy et al., 2018). Interestingly, under our conditions, we found an enrichment of K560 in the MT pellet in the presence compared to the absence of KBD (75.1 ± 7.1 % *vs.* 46.6 ± 3.9 % of K560 in the MT pellet in the presence *vs.* the absence of KBD, respectively; $n= 3$; $P = 0.0037$). In addition, we

found that KBD was apparent in the MT pellet only in the presence of K560, but not in its absence (59.7 ± 10.6 % vs. 2.0 ± 1.7 % of KBD in the MT pellet in the presence vs. the absence of K560, respectively; $n= 3$; $P = 0.0007$), suggesting these two proteins form a complex that exhibits a higher affinity for MTs. Altogether, our data indicate that KBD is able to recruit enough Kinesin-1 to MTs both *in vitro* and *in vivo*. This recruitment is sufficient to rescue centrosome separation defects in neuroblast, but not correct transport in oocyte, suggesting that the need for Kinesin-1 recruitment to microtubules depends on the cellular context.

Discussion.

Full-length Ensconsin/MAP7 is required for maintaining mitotic spindle size.

Ensconsin/MAP7 was first discovered two decades ago and was originally purified from microtubule pellets isolated from epithelial cells (Bulinski and Bossler, 1994). Preliminary overexpression experiments did not reveal modified microtubule dynamics in human interphase cells, and *ensc* mutant *Drosophila* oocytes have normal MT cytoskeletons (Faire et al., 1999). However, changes in *Ensc*/MAP7 levels affect spindle morphogenesis in fly neural stem cells and in human cultured cells to prevent spindle defects (Bulinski et al., 2001; Gallaud et al., 2014; McHedlishvili et al., 2018). Fly *ensc* mutant NBs display short spindles and have reduced MT polymerization speeds. In addition, Ensconsin strongly stimulates MT polymerization *in vitro*, and its overexpression increases spindle length (Figure S1). Rescue experiments indicate that neither MBD-GFP nor KBD-GFP fusion proteins are able to restore spindle length, even when expressed at similar levels to full-length Ensconsin-GFP, which efficiently rescues that phenotype. This reveals that although it has a functional MT-binding sequence, the MBD is not able to stimulate MT polymerisation on its own *in vivo*. Further studies at the molecular level will be needed to investigate how the MBD and KBD domains cooperate to stimulate MT polymerisation.

Mechanisms of Ensconsin/MAP7 stimulation of Kinesin-1 recruitment to MTs

Several studies have shown a functional connection between Kinesin-1 and Ensconsin. First of all, inhibition of Ensconsin and Kinesin-1 have yielded similar phenotypes in four different studies (Barlan et al., 2013; Gallaud et al., 2014; Metzger et al., 2012; Sung et al., 2008). Second, both proteins co-localizes on the internal MT network of *Drosophila* oocyte egg chambers (Sung et al., 2008), this paper). Third, Ensconsin C-terminal domain (KBD) and Kinesin-1 can interact *in vivo* ((Hooikaas, 2018; Metzger et al., 2012) this study). Based on the current literature, the recruitment model suggests that Ensconsin bound to the MT lattice (via the MBD) serves as a direct recruitment platform for Kinesin-1 (Figure 5C). This targeting model is supported by Kinesin-1 motor recruitment on MTs, which is lower in *ensc* oocyte extracts and undetectable in intact *ensc* oocytes (Sung et al., 2008), this study, and Figure 4). Furthermore, in Ensconsin and Kinesin-1 knockdown muscle cells, a fusion protein between the *Ensc*-MBD and Kinesin-1 motor domain (leading to strong recruitment of Kinesin motor to the MT network) was able to rescue nuclei spacing, thus strongly supporting that the function of Ensconsin is to deliver Kinesin-1 to MTs (Metzger et al., 2012). Interestingly, this targeting model of Kinesin-1 by MAP7 seems to be required to promote branch formation in rat neurones but not essential for axon growth (Tymanskyj et al., 2018). Finally, this direct recruitment platform model is supported *in vitro*, as the Kinesin-1 motor is strongly recruited on Ensconsin-labelled MTs (Monroy et al., 2018), Figure 5). Our study shows that an additional level of regulation comes into play. In fly NBs, Ensconsin and Kinesin-1 are jointly involved in the centrosome separation process (Gallaud et al., 2014). As shown here, this defective centrosomal separation phenotype is completely restored by the simple expression of KBD, independently of microtubules, since we show that KBD does not have the property of binding microtubules. These results confirm the ability of KBD to activate Kinesin-1 in S2 cells and in rat neurones (Barlan et al., 2013; Tymanskyj et al., 2018). This activation is supported by the fact that the KBD/Kinesin-1 motor complex can stimulate the binding of Kinesin-1 to MTs *in vitro* and *in vivo* (figure model 5E, panel b). We believe that this stimulation of the motor binding can occur in solution because we were not able to detect any association of the KBD with MTs either *in vivo* or *in vitro*, as also recently shown by other groups using rat and human Ensconsin/MAP7 (Hooikaas, 2018; Tymanskyj et al., 2018). Interestingly, this interaction between Ensconsin and KHC is observed in cell extracts, with or without polymerised microtubules (this work). Intra-molecular auto-inhibition has already been documented through interaction between the motor domain and the tail domain of KHC (Verhey et al., 2011). However, the interaction domain between Ensconsin and

Kinesin-1 has been mapped on a different domain on the stem of the *Drosophila* Kinesin-1 stalk, a domain that has not been so far described to exert any self-inhibiting properties on the motor domain. It is possible, as suggested by other groups, that this self-inhibition may be relieved after binding to the KBD of Ensconsin/MAP7 (Hooikaas, 2018; Monroy et al., 2018), see model Figure 5). The relief of inhibition is probably a very transient phenomenon and the dis-inhibited form of Kinesin-1 has to quickly find a microtubule to land before returning to the auto-inhibited form. This ephemeral interaction between Ensconsin and Kinesin-1 is certainly critical because Ensconsin is strongly anchored on MTs and a strong interaction with Kinesin-1 would impair subsequent Kinesin-1 movement and probably the jump between crossing MTs, an event proposed to trigger branch formation in neurones (Tymanskyj et al., 2018). Altogether, it will be interesting to examine in the future how these auto-inhibition domains cooperate to regulate Kinesin-1 function in space and time.

On the other hand, this full rescue of Kinesin-1 function is not validated in *ensc* mutant oocytes: The KBD expression only favours a partial localization of Gurken and Staufen. Interestingly, a recent study have demonstrated that Staufen targeting to the posterior pole is a two-step Kinesin-1 dependent process that occurs during stage 9 and 10B of oogenesis. During stage 9, Staufen particles are transported via Kinesin-1 on the polarised MT network which plus ends point toward the posterior pole where these particles are anchored by Myosin V. During stage 10B, the polarised MT network is completely reorganised, and Kinesin-1 MT sliding occurs between cytoplasmic bundles and stable cortically anchored MTs. This sliding is responsible for the very fast streaming of Staufen particles that are captured at the posterior pole. These two modes of transport are required for full Staufen delivery (Lu et al., 2018). Interestingly, KBD was able to support 75 % of WT Kinesin-1 mediated transport of Staufen at stage 9 but was largely inefficient for ooplasm streaming at stage 10B. Our hypothesis is that Kinesin-1 demand during stage 9 is low suggesting, similarly to centrosome separation in NBs, and that a weak targeting of Kinesin-1 targeting to the polarised MT arrays by KBD is sufficient for biased transport toward the cortex. Oocyte streaming and MT organisation at stage 10B probably requires much more Kinesin-1 targeting to the MT network which can not be supported by the KBD alone (Serbus et al., 2005).

Altogether, it is important to keep in mind that the KBD is not expressed in normal fly cells and Ensconsin exist as a whole entity. However, our rescue experiments have allowed us to reveal a moderate but physiologically relevant property of KBD to target Kinesin-1 to the microtubule network *in vivo* and *in vitro*. We believe that MT-bound Ensconsin provides a platform to simultaneously recruit and transiently stimulate Kinesin-1 binding to MTs (Figure

5E, panel c). The Ensconsin/MAP7 family of proteins can therefore be considered as “Microtubule-tethered Kinesin-1 activators” (Hooikaas, 2018). Remarkably, our data suggest that the model based on high Kinesin-1 targeting on MTs by full length Ensconsin is not an absolute requirement for development, since KBD flies are viable. This confirms the idea that only a small amount of Kinesin-1 targeting MTs is sufficient to support fly development, at least under laboratory conditions where animals are maintained. However, unlike the flies saved by the full-length Ensconsin, KBD females remain sterile, perhaps because in addition to oocyte polarisation defects, the *ensc* mutant meiotic spindle is abnormal and does not support correct chromosome segregation (Personal communication, Professor Ohkura, University of Edinburgh). In flies, the observed weak targeting of Kinesin-1 on the MT network by KBD is sufficient to sustain Kinesin-1 function in S2 cells, neuroblasts, stage oocytes 9 but not in stage 10B oocytes (Barlan et al., 2013). However, even if the size factor is the first thing that comes to mind when comparing these four cell types, we cannot rule out the hypothesis that the observed recruitment differences are also dependent on other levels of regulation. We cannot exclude, as observed for other MAPs, that Kinesin-1 affinity for the microtubule is also directly related to the presence of particular isoforms of tubulins or under the control of the tubulin code that could vary between cells (Yu et al., 2015). Further studies will be needed to understand how the optimal targeting of Kinesin-1 by Ensconsin on microtubules is achieved according to different cell types.

Acknowledgments.

This work was funded by the Ligue Nationale Contre le Cancer, the Fondation ARC pour la recherche sur le cancer. M. M. is a doctoral fellow of the Région Bretagne and the Ligue Nationale contre le Cancer. E. G. was a doctoral fellow of the Région Bretagne. R. C was a doctoral fellow of the French Ministry of Research. AG was supported by the CNRS and by the Fondation ARC pour la recherche sur le cancer (grant PJA 20161204931). KMOM is supported by the NIH (R00HD080981), the March of Dimes Foundation, and the Simons Foundation. We would like to thank R. Basto for the kind gift of RFP-tubulin expressing flies. We thank Kahina Sadaouli for the preliminary functional analyses of Ensconsin domains during oocyte development. We thank the Microscopy Rennes Imaging Center for the microscopy facilities. We thank Christelle Benaud, Romain Gibeaux and Denis Chrétien for critical reading and helpful comments on the manuscript. The authors have no competing financial interests to declare.

References

- Barlan, K. and Gelfand, V. I.** (2017). Microtubule-Based Transport and the Distribution, Tethering, and Organization of Organelles. *Cold Spring Harb Perspect Biol* **9**.
- Barlan, K., Lu, W. and Gelfand, V. I.** (2013). The Microtubule-Binding Protein Ensconsin Is an Essential Cofactor of Kinesin-1. *Curr Biol*.
- Brendza, R. P., Serbus, L. R., Duffy, J. B. and Saxton, W. M.** (2000). A function for kinesin I in the posterior transport of oskar mRNA and Staufén protein. *Science* **289**, 2120-2.
- Brendza, R. P., Serbus, L. R., Saxton, W. M. and Duffy, J. B.** (2002). Posterior localization of dynein and dorsal-ventral axis formation depend on kinesin in *Drosophila* oocytes. *Curr Biol* **12**, 1541-5.
- Bulinski, J. C. and Bossler, A.** (1994). Purification and characterization of ensconsin, a novel microtubule stabilizing protein. *J Cell Sci* **107** (Pt 10), 2839-49.
- Bulinski, J. C., Odde, D. J., Howell, B. J., Salmon, T. D. and Waterman-Storer, C. M.** (2001). Rapid dynamics of the microtubule binding of ensconsin in vivo. *J Cell Sci* **114**, 3885-97.
- Castoldi, M. and Popov, A. V.** (2003). Purification of brain tubulin through two cycles of polymerization-depolymerization in a high-molarity buffer. *Protein Expr Purif* **32**, 83-8.
- Conduit, P. T. and Raff, J. W.** (2010). Cnn dynamics drive centrosome size asymmetry to ensure daughter centriole retention in *Drosophila* neuroblasts. *Curr Biol* **20**, 2187-92.
- Djagaeva, I., Rose, D. J., Lim, A., Venter, C. E., Brendza, K. M., Moua, P. and Saxton, W. M.** (2012). Three routes to suppression of the neurodegenerative phenotypes caused by kinesin heavy chain mutations. *Genetics* **192**, 173-83.
- Duncan, J. E. and Warrior, R.** (2002). The cytoplasmic dynein and kinesin motors have interdependent roles in patterning the *Drosophila* oocyte. *Curr Biol* **12**, 1982-91.
- Faire, K., Waterman-Storer, C. M., Gruber, D., Masson, D., Salmon, E. D. and Bulinski, J. C.** (1999). E-MAP-115 (ensconsin) associates dynamically with microtubules in vivo and is not a physiological modulator of microtubule dynamics. *J Cell Sci* **112** (Pt 23), 4243-55.
- Ferrandon, D., Elphick, L., Nusslein-Volhard, C. and St Johnston, D.** (1994). Staufén protein associates with the 3'UTR of bicoid mRNA to form particles that move in a microtubule-dependent manner. *Cell* **79**, 1221-32.
- Gallaud, E., Caous, R., Pascal, A., Bazile, F., Gagne, J. P., Huet, S., Poirier, G. G., Chretien, D., Richard-Parpaillon, L. and Giet, R.** (2014). Ensconsin/Map7 promotes microtubule growth and centrosome separation in *Drosophila* neural stem cells. *J Cell Biol* **204**, 1111-21.
- Giet, R., McLean, D., Descamps, S., Lee, M. J., Raff, J. W., Prigent, C. and Glover, D. M.** (2002). *Drosophila* Aurora A kinase is required to localize D-TACC to centrosomes and to regulate astral microtubules. *J Cell Biol* **156**, 437-51.
- Heald, R. and Khodjakov, A.** (2015). Thirty years of search and capture: The complex simplicity of mitotic spindle assembly. *J Cell Biol* **211**, 1103-11.
- Hooikaas, J., M., Martin, G., Kuijntjes, C. Peeters, E. Katrukha, L., Ferrari, R., Stucchi, D., Verhagen, W., van Riel, A., Maarten Altelaar, C., Hoogenraad, S., Rüdiger, L., Kapitein and A., Akhmanova.** (2018). MAP7 family proteins are microtubule-tethered allosteric activators of kinesin-1. *BioRxiv*.

Januschke, J., Gervais, L., Dass, S., Kaltschmidt, J. A., Lopez-Schier, H., St Johnston, D., Brand, A. H., Roth, S. and Guichet, A. (2002). Polar transport in the *Drosophila* oocyte requires Dynein and Kinesin I cooperation. *Curr Biol* **12**, 1971-81.

Januschke, J., Gervais, L., Gillet, L., Keryer, G., Bornens, M. and Guichet, A. (2006). The centrosome-nucleus complex and microtubule organization in the *Drosophila* oocyte. *Development* **133**, 129-39.

Januschke, J., Llamazares, S., Reina, J. and Gonzalez, C. (2011). *Drosophila* neuroblasts retain the daughter centrosome. *Nat Commun* **2**, 243.

Lu, W., Lakonishok, M., Serpinskaya, A. S., Kirchenbuechler, D., Ling, S. C. and Gelfand, V. I. (2018). Ooplasmic flow cooperates with transport and anchorage in *Drosophila* oocyte posterior determination. *J Cell Biol* **217**, 3497-3511.

Lu, W., Winding, M., Lakonishok, M., Wildonger, J. and Gelfand, V. I. (2016). Microtubule-microtubule sliding by kinesin-1 is essential for normal cytoplasmic streaming in *Drosophila* oocytes. *Proc Natl Acad Sci U S A* **113**, E4995-5004.

McHedlishvili, N., Matthews, H. K., Corrigan, A. and Baum, B. (2018). Two-step interphase microtubule disassembly aids spindle morphogenesis. *BMC Biol* **16**, 14.

Metzger, T., Gache, V., Xu, M., Cadot, B., Folker, E. S., Richardson, B. E., Gomes, E. R. and Baylies, M. K. (2012). MAP and kinesin-dependent nuclear positioning is required for skeletal muscle function. *Nature* **484**, 120-4.

Mitchison, T. and Kirschner, M. (1984). Dynamic instability of microtubule growth. *Nature* **312**, 237-42.

Monroy, B. Y., Sawyer, D. L., Ackermann, B. E., Borden, M. M., Tan, T. C. and Ori-McKenney, K. M. (2018). Competition between microtubule-associated proteins directs motor transport. *Nat Commun* **9**, 1487.

Neuman-Silberberg, F. S. and Schupbach, T. (1993). The *Drosophila* dorsoventral patterning gene *gurken* produces a dorsally localized RNA and encodes a TGF alpha-like protein. *Cell* **75**, 165-74.

Palacios, I. M. and St Johnston, D. (2002). Kinesin light chain-independent function of the Kinesin heavy chain in cytoplasmic streaming and posterior localisation in the *Drosophila* oocyte. *Development* **129**, 5473-85.

Rebollo, E., Sampaio, P., Januschke, J., Llamazares, S., Varmark, H. and Gonzalez, C. (2007). Functionally unequal centrosomes drive spindle orientation in asymmetrically dividing *Drosophila* neural stem cells. *Dev Cell* **12**, 467-74.

Rusan, N. M. and Peifer, M. (2007). A role for a novel centrosome cycle in asymmetric cell division. *J Cell Biol* **177**, 13-20.

Serbus, L. R., Cha, B. J., Theurkauf, W. E. and Saxton, W. M. (2005). Dynein and the actin cytoskeleton control kinesin-driven cytoplasmic streaming in *Drosophila* oocytes. *Development* **132**, 3743-52.

St Johnston, D., Beuchle, D. and Nusslein-Volhard, C. (1991). *Staufen*, a gene required to localize maternal RNAs in the *Drosophila* egg. *Cell* **66**, 51-63.

Sung, H. H., Telley, I. A., Papadaki, P., Ephrussi, A., Surrey, T. and Rorth, P. (2008). *Drosophila* *ensconsin* promotes productive recruitment of Kinesin-1 to microtubules. *Dev Cell* **15**, 866-76.

Tymanskyj, S. R., Yang, B. H., Verhey, K. J. and Ma, L. (2018). MAP7 regulates axon morphogenesis by recruiting kinesin-1 to microtubules and modulating organelle transport. *Elife* **7**.

Verhey, K. J., Kaul, N. and Soppina, V. (2011). Kinesin assembly and movement in cells. *Annu Rev Biophys* **40**, 267-88.

Walczak, C. E. and Heald, R. (2008). Mechanisms of mitotic spindle assembly and function. *Int Rev Cytol* **265**, 111-58.

Yu, I., Garnham, C. P. and Roll-Mecak, A. (2015). Writing and Reading the Tubulin Code. *J Biol Chem* **290**, 17163-72.

Figures.

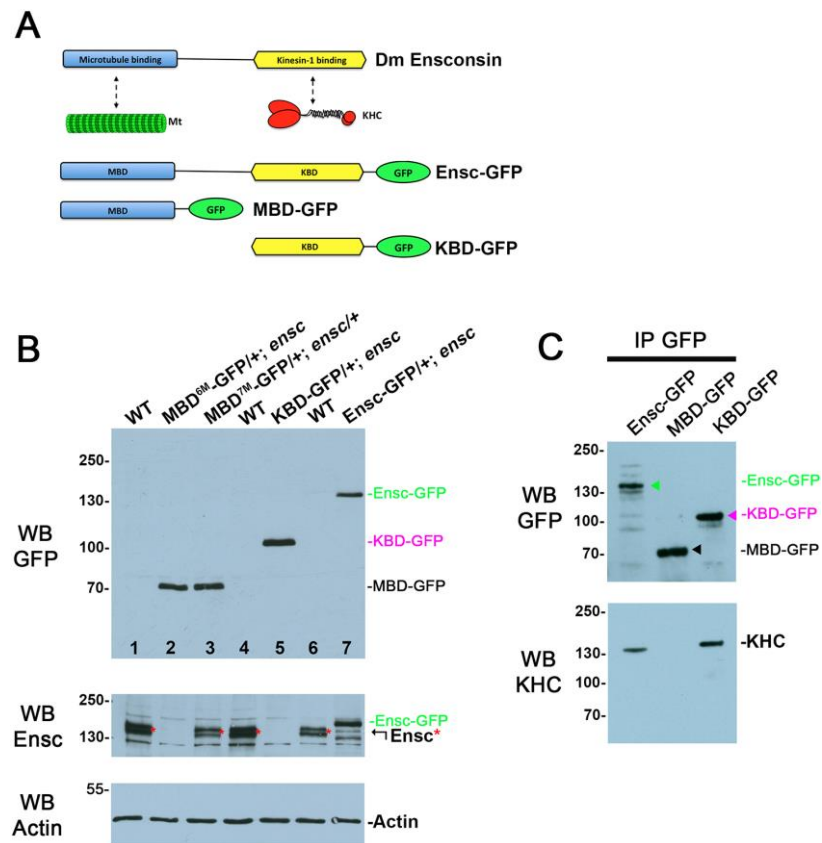


Figure 1. Schematic diagram and expression of GFP-tagged Ensconsin variants.

A) Endogenous Ensconsin harbours an N-terminal MT-binding domain (MBD, blue) and a C-terminal Kinesin-binding domain (KBD, yellow). The three proteins were tagged with GFP and expressed in *ensc*-null flies using a poly ubiquitin promoter. B) Western blot analysis of different GFP-tagged Ensconsin variants from brain tissue. The whole membrane was probed with GFP antibodies for Western blotting (top). The same membrane was subsequently stripped (see Methods) to reveal endogenous Ensconsin (middle) and an Actin loading control (bottom). WT: control brain tissue (lanes 1, 4, 6). The expression of the transgenes is shown in *ensc*-null individuals (lanes 2, 5, 7), except in lane 3 where a MBD-GFP line is examined in hemizygous *ensc* tissue. The endogenous Ensconsin band/doublet is indicated with a red asterisk (middle panel). C) Whole fly extracts were prepared and subjected to immunoprecipitation using GFP-TRAP beads (see methods). The beads were then analysed by Western blotting and probed with an anti-GFP (top) or anti-KHC (bottom) antibodies. The positions of MBD-GFP, KBD-GFP and Ensc-GFP are indicated on the right with dark, pink and green arrowheads respectively. KHC is present in Ensc-GFP and KBD-GFP but not in MBD-GFP immunoprecipitates.

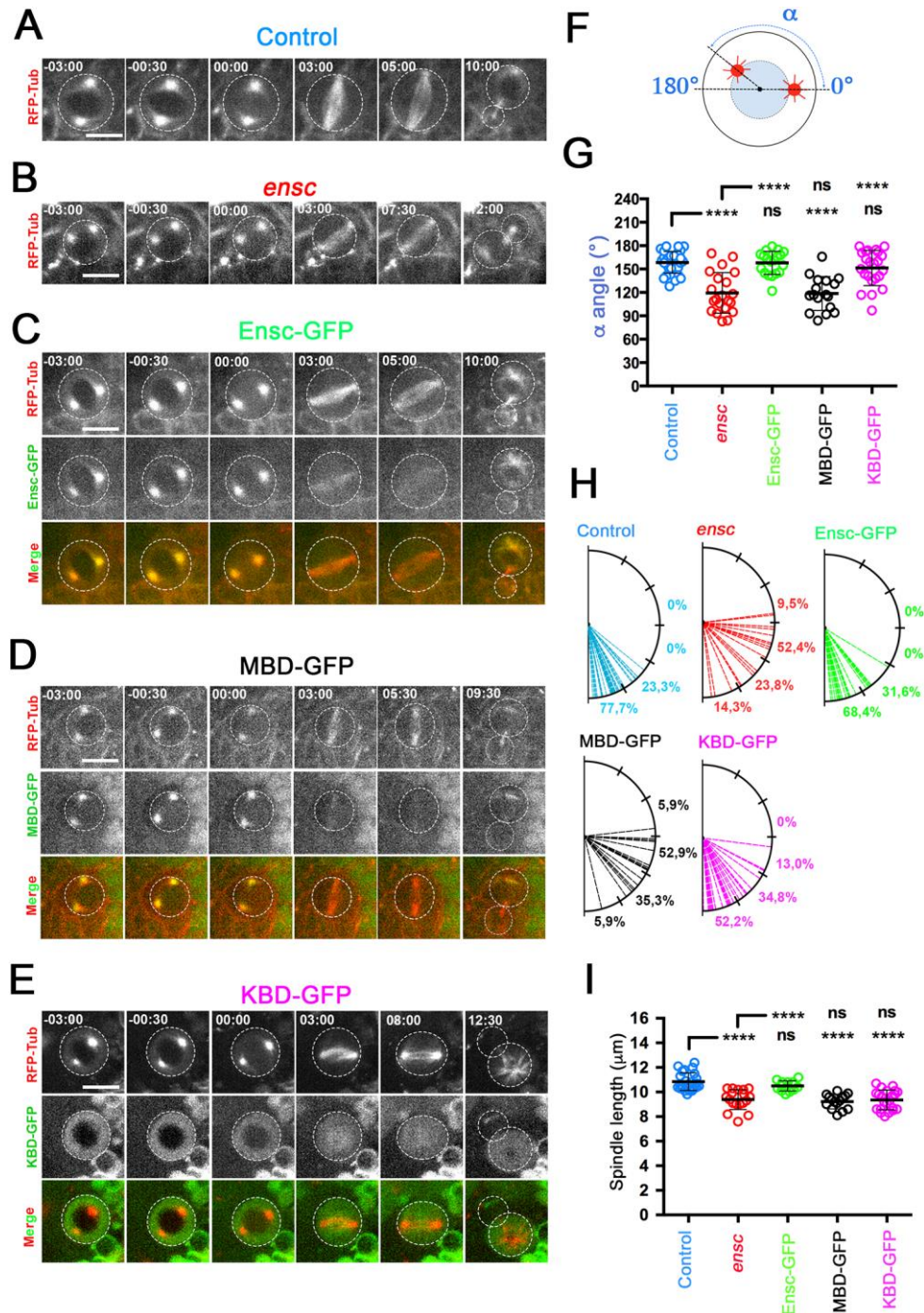


Figure 2. Functional analysis of Enscins microtubule- and Kinesin-binding domains during cell division.

A) Selected frames of a control NB and B) a mutant *ensc* NB expressing RFP-tubulin during cell division. Thirty seconds before the nuclear envelope breakdown (NEBD), the centrosomes are already fully separated and well positioned in WT cells, but not in *ensc*. C) *ensc* mutant NB expressing Ensc-GFP during cell division. In the merge pictures in C-E, RFP-tubulin (RFP-Tub) is red and GFP-tagged proteins are green, while they are both monochrome in the upper and middle panels, respectively. D) *ensc* mutant NB expressing

MBD-GFP during cell division. Here, the centrosomes are incompletely separated before NEBD. E) *ensc* mutant NB expressing KBD-GFP during cell division. Note that this particular cell was isolated from flattened brains in PBS to reveal that KBD-GFP does not co-localize with the MT cytoskeleton. The centrosome separation defect is fully restored. Scale bars: 10 μm . F) Scheme showing the α angle measurement, reflecting centrosome separation for the indicated genotypes (see Methods). G) Box plot (\pm s.d.) showing the mean centrosome separation α angle for control ($158.5 \pm 14.0^\circ$, $n=30$), *ensc* ($119.4 \pm 26.0^\circ$, $n=21$), *Ensc*-GFP ($157.9 \pm 14.9^\circ$, $n=19$), MBD-GFP ($118.6 \pm 21.8^\circ$, $n=12$), and KBD-GFP ($151.3 \pm 22.6^\circ$, $n=23$) NBs. H) Representation of the α angle distributions of the NBs shown in panel G. I) Box plot (\pm s.d.) showing the mitotic spindle length for control ($10.9 \pm 0.7 \mu\text{m}$, $n=24$), *ensc* ($9.4 \pm 0.8 \mu\text{m}$, $n=18$), *Ensc*-GFP ($10.5 \pm 0.4 \mu\text{m}$, $n=13$), MBD-GFP ($9.2 \pm 0.6 \mu\text{m}$, $n=12$), and KBD-GFP ($9.3 \pm 0.8 \mu\text{m}$, $n=22$) NBs. *****, $P < 0.0001$ (Wilcoxon test).

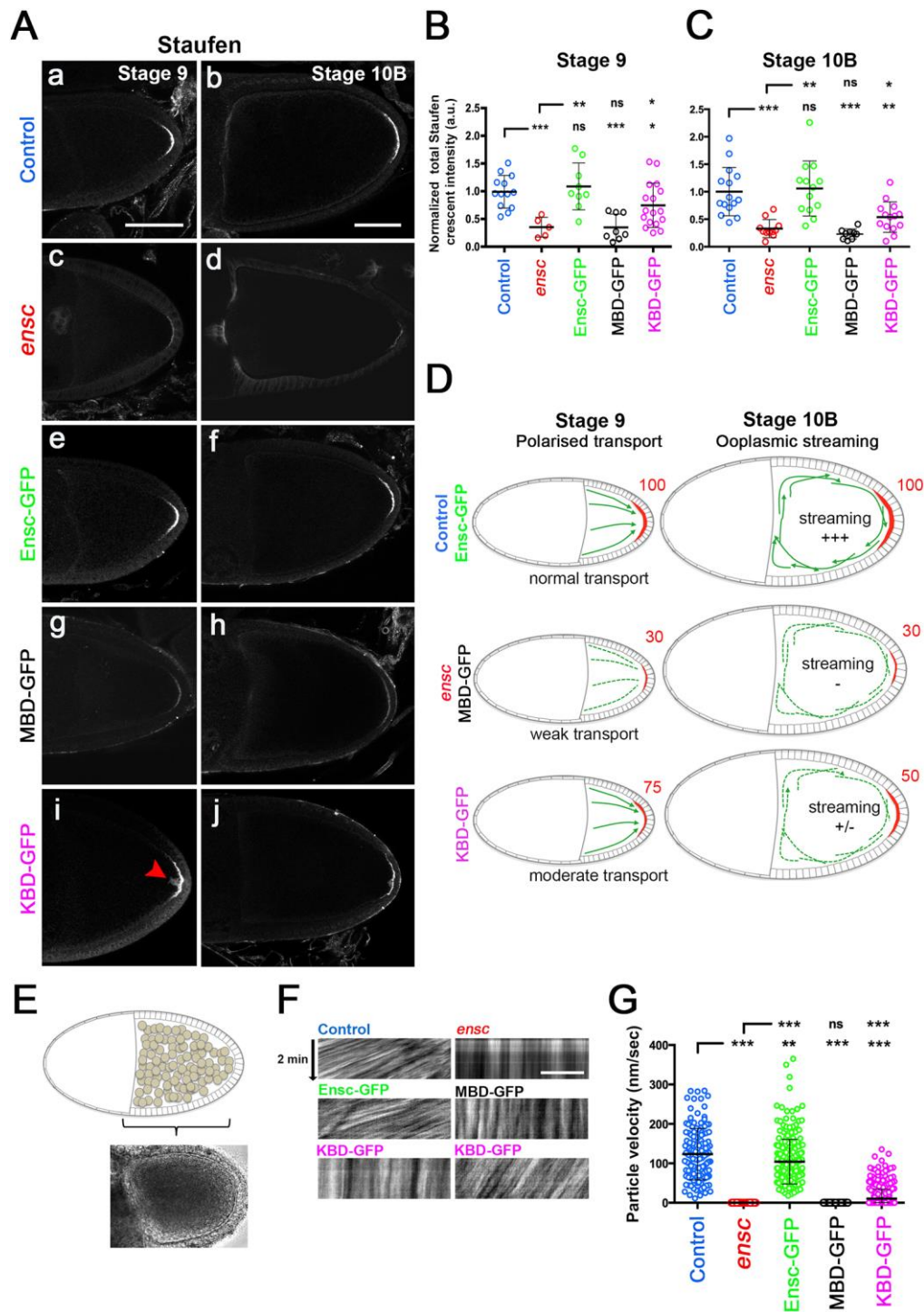


Figure 3. The Kinesin-binding domain of Ensconsin is not sufficient to restore the Staufen localizations in the oocyte egg chamber and fast oocyte streaming.

A) Stage 9 control (a), *ensc* (c), and *ensc* mutant fly oocytes expressing full-length Ensconsin-GFP (e), MBD-GFP (g) or KBD-GFP (i) were stained for Staufen. Stage 10B oocytes from the same five genotypes were stained for Staufen (b-j). The red arrow in panel i points defective Staufen localization. B) Box plot showing the quantification of Staufen crescent

intensity (\pm s.d.) during stage 9. WT (1 ± 0.29 , $n=13$), *ensc* (0.35 ± 0.18 , $n=5$), Ensc-GFP (1.08 ± 0.42 , $n=9$), MBD (0.35 ± 0.24 , $n=8$) and *ensc* ; KBD (0.74 ± 0.40 , $n=17$). The red arrow in C) Box plot showing the quantification of Staufen crescent intensity (\pm s.d.) at stage 10B. WT (1.0 ± 0.44 , $n=15$), *ensc* (0.33 ± 0.16 , $n=11$), Ensc-GFP (1.06 ± 0.50 , $n=13$) MBD (0.23 ± 0.09 , $n=9$), KBD (0.54 ± 0.28 , $n=14$). D) Schematic view of Staufen transport to the posterior cortex during stage 9 (left) and 10B (right). The Staufen crescent is displayed in red. The microtubule network (in green) is polarised at stage 9 and the arrows indicates the direction of the MT plus ends. Dotted green lines indicate altered Kinesin-1 transport. The Kinesin-1 mediated-polarised transport of Staufen to the posterior cortex is strongly diminished in MBD and *ensc* oocyte but fully rescued by expression of Ensc-GFP. Expression of KBD is able to rescue 75% of Staufen targeting to the posterior cortex. During stage 10B (top right), a complete reorganisation of the MT network occurs. Kinesin-1 mediated MT sliding leads to cytoplasmic mixing of the ooplasm, a process that also contributes to Staufen targeting. Staufen crescent formation is fully rescued by Ensc-GFP, moderately impaired in KBD oocytes while *ensc* and MBD oocytes display a weak Staufen crescent.

E) Scheme of an oocyte (left) and phase contrast image of a control oocyte egg chamber (right) where particles are visible. Scale bar: 50 μ m. F) Kymographs showing the displacement of particles from different ooplasm for 2 minutes. Scale Bar: 10 μ m. The genotype is indicated at the top of each image. Control ($n=11$, Top left panel) and Ensc-GFP ($n=16$, middle left panel) expressing oocytes show similar particle velocities. *ensc* oocytes ($n=15$, top right panel) and MBD-GFP oocytes ($n=13$, middle right panel) do not show any ooplasmic streaming. Note that KBD ($n=23$) oocytes show either absent (17/23, bottom left panel) or slower ooplasmic streaming (6/23, bottom right panel). G) Scatter dot plot showing the mean particle velocities (\pm s.d) of control ($n=146$, 123 ± 65 nm/sec), Ensc-GFP (104 ± 56 nm/sec, $n=243$), KBD-GFP ($n=395$, 10 ± 23 nm/sec), MBD-GFP (0 nm/sec, $n=195$) or *ensc* (0 nm/sec, $n=225$) ooplasm. *: $P < 0.01$, **: $P < 0.001$ ***: $P < 0.0001$, Wilcoxon test.

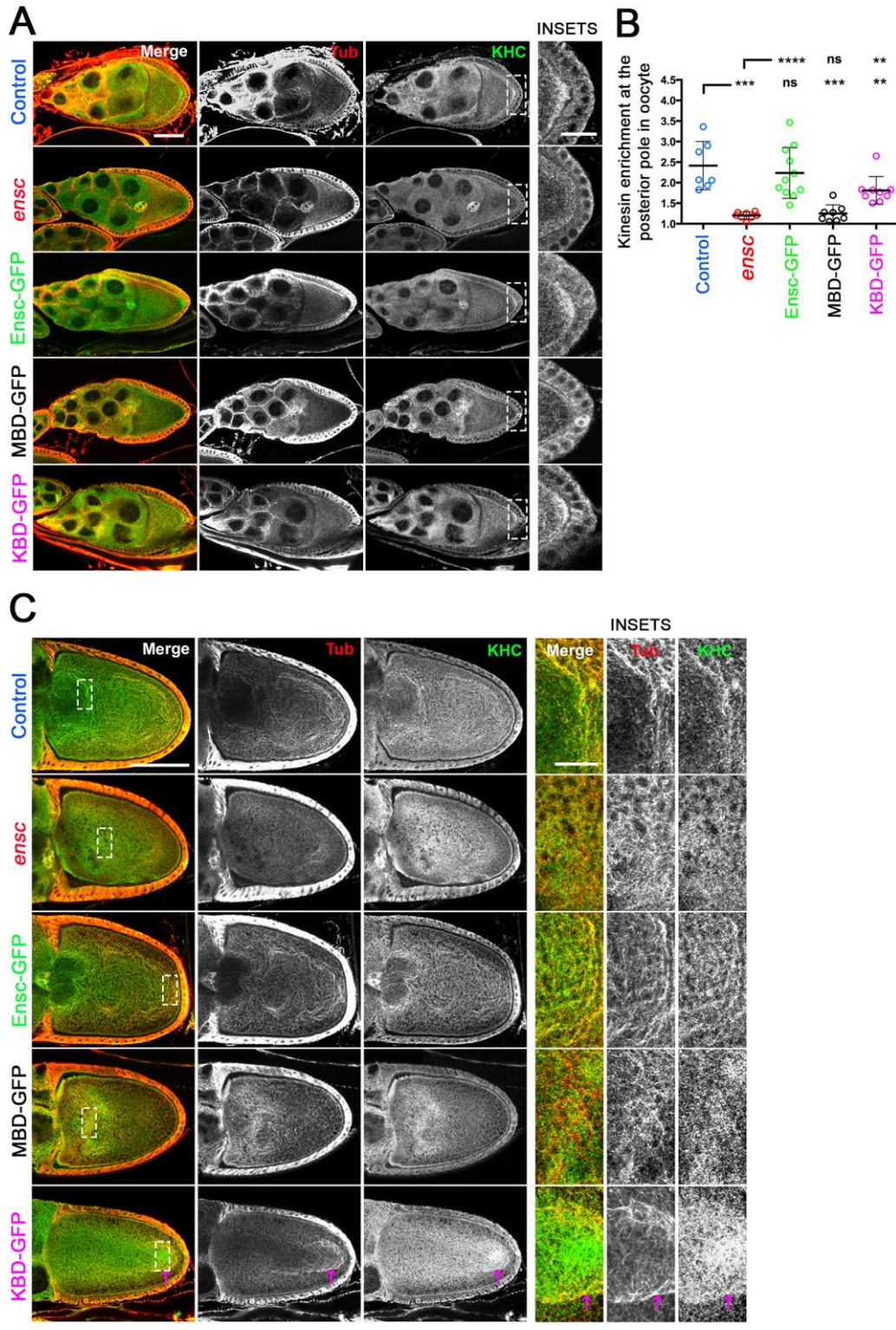


Figure 4: The Enscinsin Kinesin-binding domain can promote minimal recruitment of Kinesin-1 on microtubules in oocytes.

A) Stage 9 oocytes of the indicated genotypes were permeabilized 1 hour, fixed and labelled with an anti-tubulin (red in the merge column, monochrome elsewhere) and an anti-Kinesin-1 antibody (green in the merge column, monochrome elsewhere). Scale bar: 50 μ m. The right part shows enlarged views of the posterior poles. Scale bar: 20 μ m. WT and Ensc-GFP shows a strong KHC labelling at the posterior side, by contrast to *ensc* or MBD-GFP oocytes where KHC is not detectable. KBD-GFP oocytes displayed diminished KHC targeting. B) Scatter dot plot showing the mean KHC recruitment (a.u \pm s.d.) at the posterior side of stage 9 oocytes. Control ($n=7$, 2.41 ± 0.59), *ensc* ($n=8$, 1.20 ± 0.59), Ensc-GFP ($n=11$, 2.24 ± 0.62), MBD-GFP ($n=8$, 1.25 ± 0.21) and KBD-GFP ($n=9$, 1.81 ± 0.34 nm/sec) ooplasm. **: $P<0.001$ ***: $P<0.0001$, Wilcoxon test. C) Stage 10B oocytes of the indicated genotypes were labelled for tubulin (red in the merge column, monochrome elsewhere) and KHC (green in the merge column, monochrome elsewhere). In control oocytes, KHC co-localizes with cytoplasmic bundles of MTs. KHC is lost from the MT network in *ensc* and MBD oocytes and appears as aggregates around the MTs of these oocytes. Ensc-GFP rescues the KHC targeting to MT bundles. Most KBD oocytes (bottom panels) display enrichment of KHC aggregates around cytoplasmic MT bundles but only few of these bundles exhibit a clear KHC labelling (pink arrow). Scale bar: 50 μ m. The right part shows enlargement views of the indicated insets, the scale bar is 20 μ m.

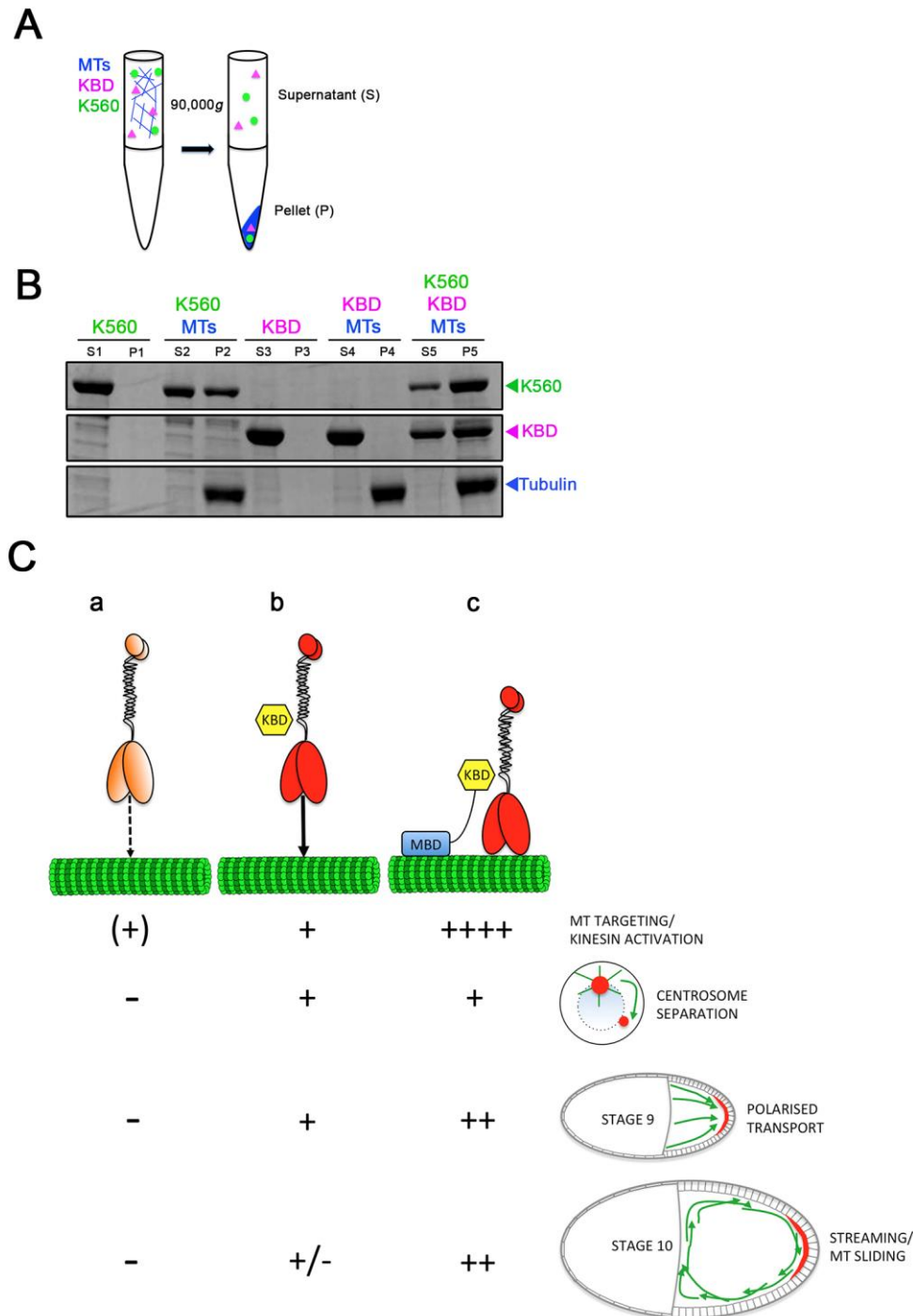


Figure 5. The Enscinsin Kinesin-binding domain can promote recruitment of K560 to MTs *in vitro*.

A) Scheme of the MT binding assay. KBD and K560, a truncated KHC protein (amino acids 1-560) were mixed in the presence of polymerized MTs and subjected to centrifugation (see Methods). MT Pellets (P) and Supernatants (S) were subsequently analysed by Western blot.

B) Coomassie-stained SDS-PAGE gel shows the binding behavior of 500 nM Ensc-KBD and/or 500 nM K560 in the presence of 2.5 μ M taxol-stabilized microtubules. Note the

increase of K560 in the MT pellet in the presence of KBD. The percentage of K560 in the MT pellet is $46.6 \pm 3.9 \%$ and $75.1 \pm 7.1\%$ in the absence and presence of Enscosin KBD respectively ($n=3$, $P=0.0036$). Enscosin KBD is detected in the MT pellet only in the presence of K560 indicating direct interaction ($59.7 \pm 10.6 \%$ vs. $2.0 \pm 1.7 \%$, $n= 3$; $P = 0.0007$).

C) Speculative Model for dual Kinesin-1 recruitment to MTs and consequences for several Kinesin-1 dependent processes in *Drosophila*. Panel a: Kinesin-1 (light orange) shows intrinsic MT binding which is weak because of auto-inhibition properties. Flies without Kinesin-1 or Enscosin cannot separate their centrosomes during interphase, and cannot perform KHC mediated transport or oocyte streaming during stage 9 and 10B of oogenesis respectively. Panel b: Our data suggest that a truncated Kinesin-1 that shows intrinsic binding to MTs can be weakly stimulated after transient interaction with KBD that may causes a relief of auto-inhibition (red). *In vivo*, this targeting of Kinesin-1 molecules to MTs is sufficient to sustain normal centrosome separation in brain NBs and almost complete Staufen mediated transport along the polarised MTs network of stage 9 oocytes, but not oocyte streaming in stage 10B of oogenesis. c: *in vivo*, MT-anchored Enscosin serves as a platform to simultaneously (i) recruit and (ii) stimulates Kinesin-1 targeting to the MTs. This dual activation is essential for efficient oocyte streaming in stage 10B oocytes.

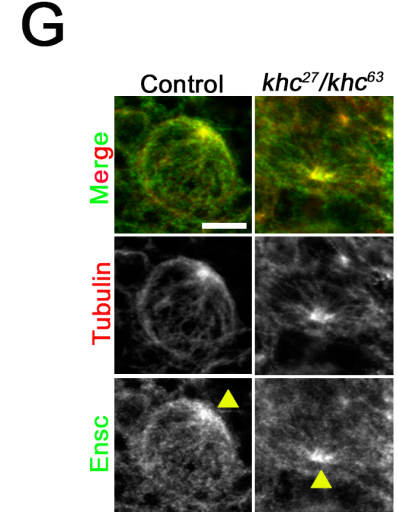
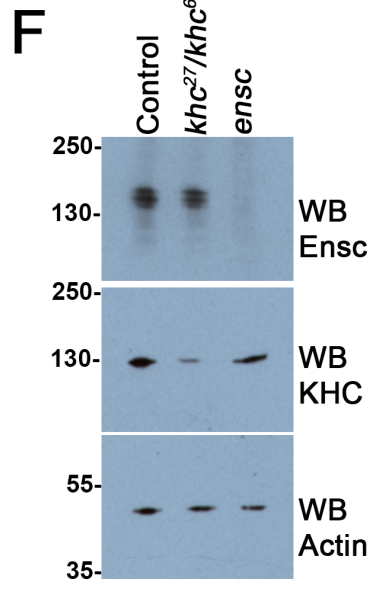
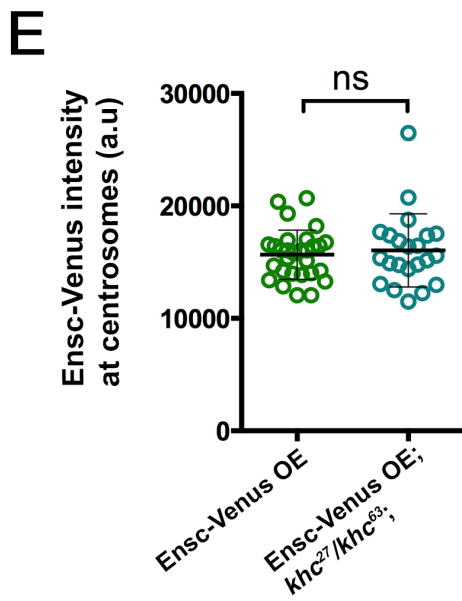
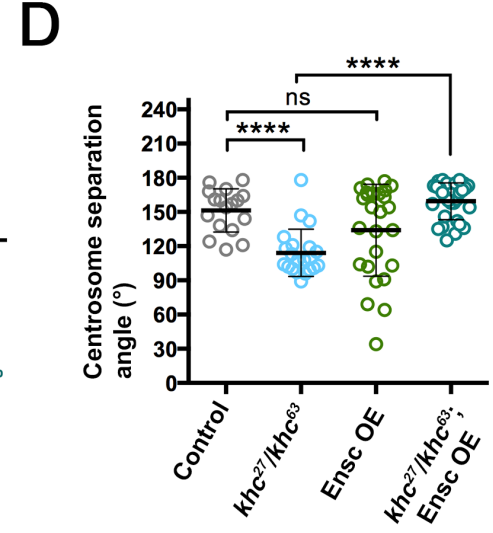
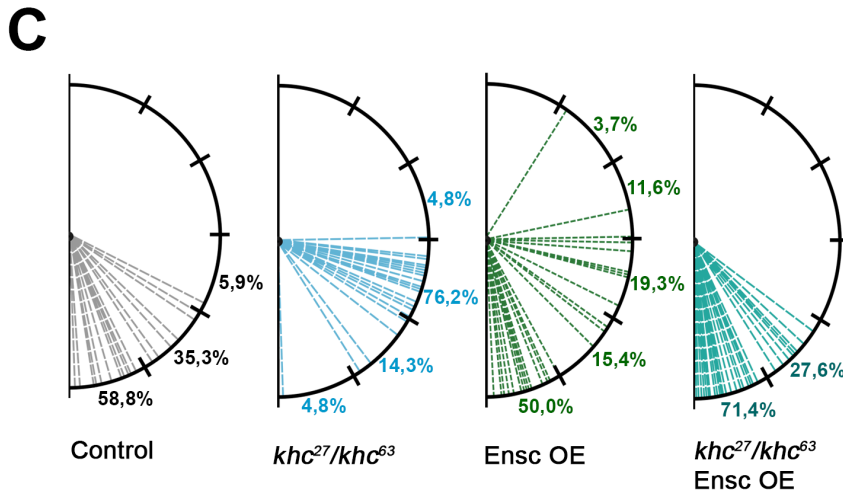
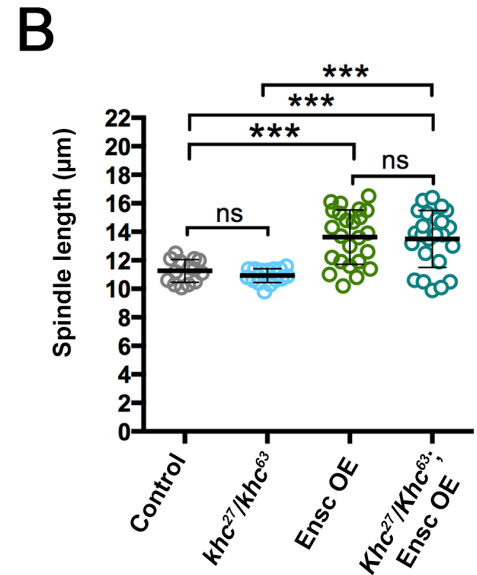
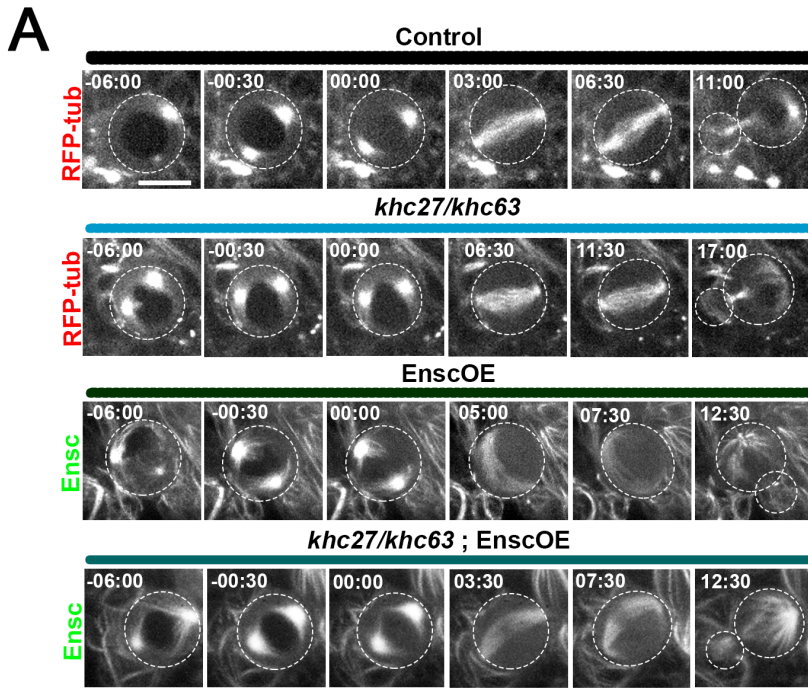


Figure S1. Overexpression of Ensconsin increases mitotic spindle length in a Kinesin-1-independent manner but efficiently rescues *khc*-dependent centrosome separation defects and in brain NBs.

A) Dividing neuroblasts were imaged in four different genotypes: control, *khc*²⁷/*khc*⁶³, Ensconsin-Venus overexpression (Encs OE) and in *khc*²⁷/*khc*⁶³ overexpressing Ensconsin (*khc*²⁷/*khc*⁶³; Encs OE). Scale bar: 10 μ m. Time is min:sec. B) Box plot showing the mean (\pm s.d.) mitotic spindle length analysis for control ($11.3 \pm 0.8 \mu\text{m}$, $n=14$), *khc*²⁷/*khc*⁶³ ($10.9 \pm 0.5 \mu\text{m}$, $n=17$), Encs OE ($13.6 \pm 1.9 \mu\text{m}$, $n=24$), *khc*²⁷/*khc*⁶³; Encs OE ($13.5 \pm 2.0 \mu\text{m}$, $n=24$) NBs. ***, $P < 0.001$ (Wilcoxon test). C) Analysis of centrosome separation angle (α) at NEBD for the indicated genotypes. D) Box plot showing the mean (\pm s.d.) centrosome separation angle for control ($151.4 \pm 19.0^\circ$, $n=17$), *khc*²⁷/*khc*⁶³ ($114.1 \pm 20.7^\circ$, $n=21$), Encs OE ($134.0 \pm 40.3^\circ$, $n=26$), *khc*²⁷/*khc*⁶³; Encs OE ($159.4 \pm 16.2^\circ$, $n=29$) NBs, corresponding to panel C. ****, $P < 0.0001$ (Wilcoxon test). E) Scatter box blot showing the mean value (\pm s.d.) of Encs-Venus centrosomal signal (a.u) 30 sec before NEBD in WT (15659 ± 2188 , $n=29$) or *khc*²⁷/*khc*⁶³ (16038 ± 3255 , $n=22$). F) Western blot showing Ensconsin, KHC and actin (as a loading control) protein levels in WT, *khc*²⁷/*khc*⁶³ mutant and *ensc* mutant brain extracts. KHC levels are stable in *ensc* mutants (and vice versa). G) Endogenous Ensconsin localization during interphase in control (left) and in *khc*²⁷/*khc*⁶³ mutant NBs (right). Tubulin is red in the merge panels and monochrome in the middle panels. Ensconsin is Green in the merge panels and Monochrome in the bottom panels. Scale bar: 5 μ m.

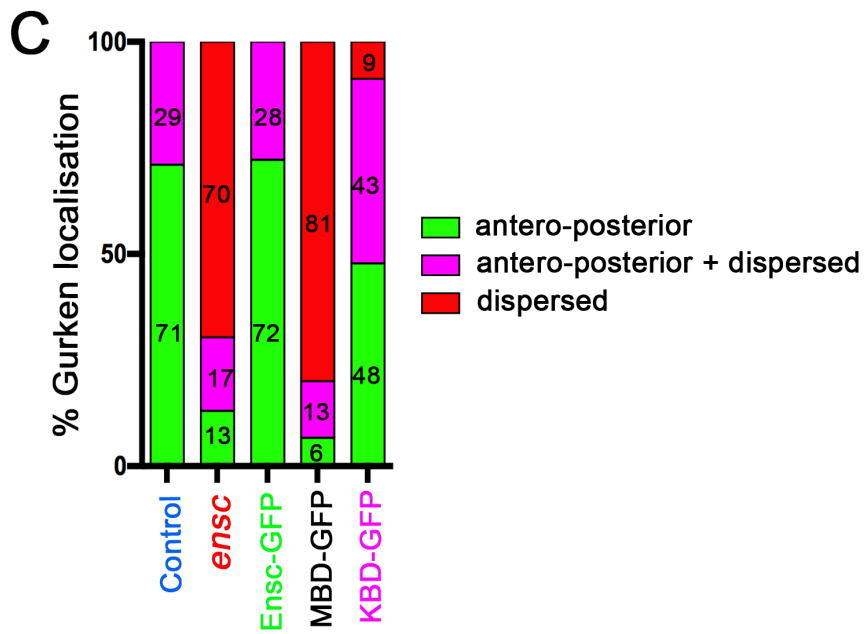
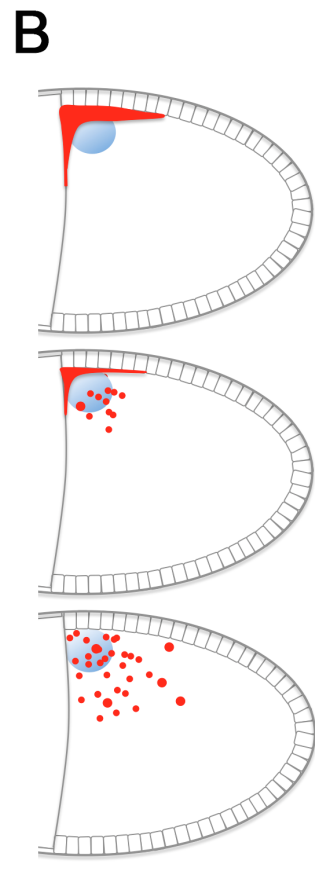
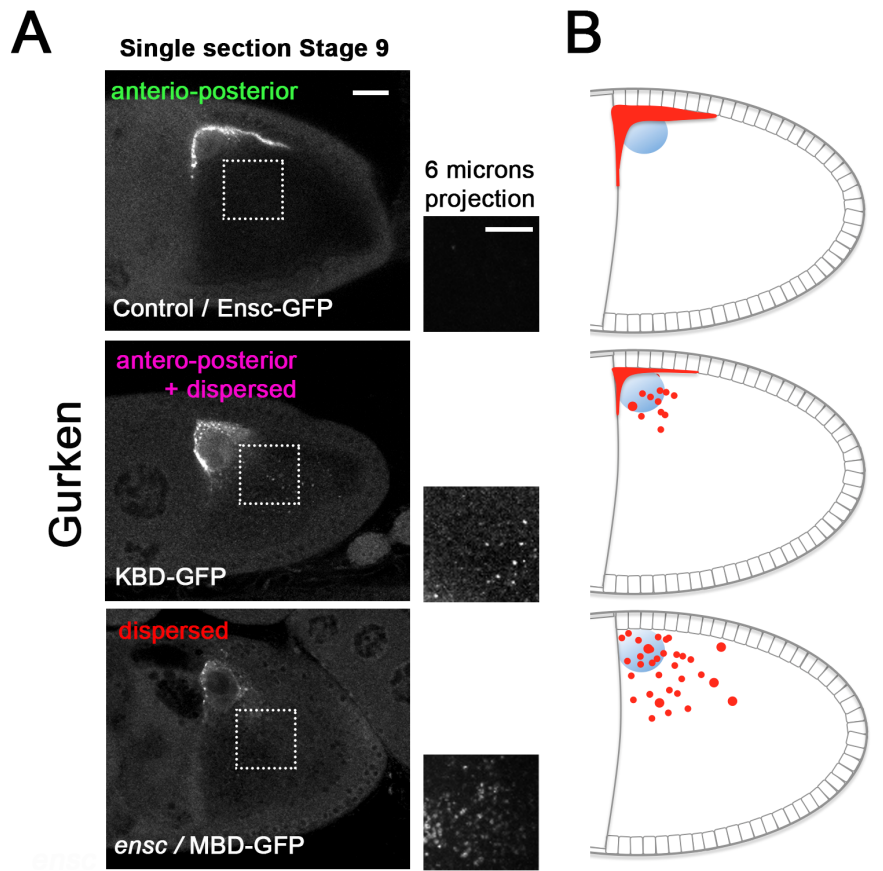


Figure S2. Gurken localization in oocytes (revoir les nombreux avec le texte)

A) Gurken localization patterns at stage 9 in different genetic backgrounds. Gurken is mainly located at the dorsal corner side of the nucleus in both control and *Ensc*-GFP. Note that it can also appear as tiny dots around the nucleus. In *ensc* and *MBD*-GFP, Gurken signal was dispersed or appeared as tiny spots around the nucleus (bottom). In *KBD*-GFP oocytes (middle), some oocytes showed a WT Gurken distribution (11/23), a small portion of the oocytes has a Gurken localization pattern comparable to *ensc* mutant (2/23) and the remaining oocytes displayed an intermediate phenotype with a punctiform distribution at the dorsal side corner region (10/23). B) Schematic diagram of Gurken localization (red) in stage 9 oocytes that summarises a representative oocyte for WT and *Ensc*-GFP (top), *KBD*-GFP (middle) and in *ensc* and *MBD*-GFP backgrounds (bottom). The nucleus is shown as blue sphere. C) Histogram showing the percentage distribution of Gurken localization in stage 9 oocytes for controls ($n=14$), *ensc* ($n=23$), *MBD*-GFP ($n=15$), *KBD*-GFP ($n=23$) and *Ensc*-GFP ($n=18$). Numbers in the columns correspond to percentages.

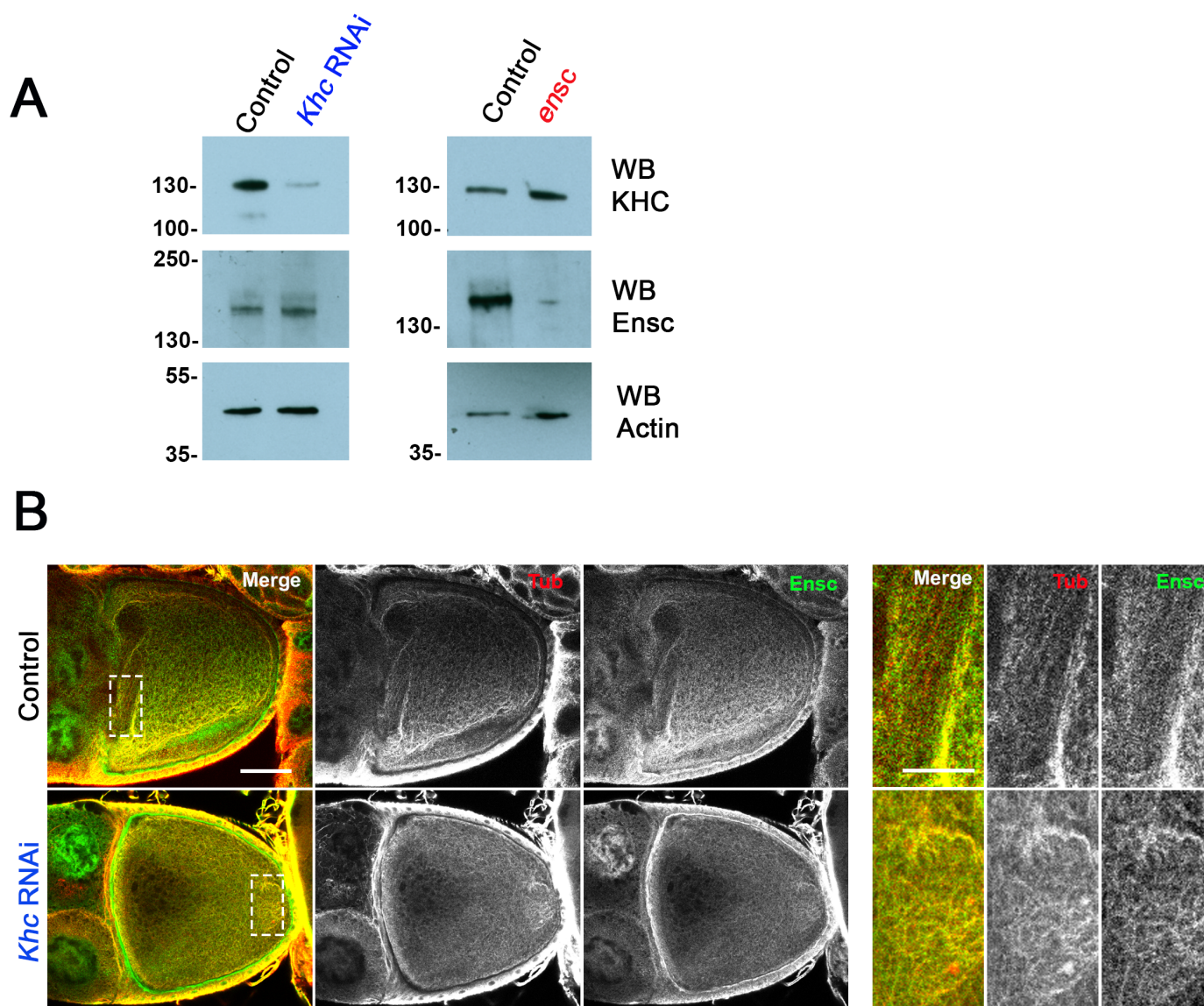


Figure S3. Ensconsin localization in *khc* RNAi oocytes and Western blot analyses.

A) Western blot showing KHC, Ensconsin and actin protein levels in control and *khc* RNAi ovary extracts (left) or in control and *ensc* mutant ovary extracts (right). B) Ensconsin (green in the merge panel and monochrome in the middle panels) and MT localization (red in green in the merge panel and monochrome in the right) panels in WT (top, n=10) and *khc* RNAi oocytes (bottom, n=12). *khc* RNAi oocytes display a loss of the large cytoplasmic MTs bundles but Ensconsin is maintained on the remaining MT cytoskeleton. Insets show an enlarged view of the cytoplasmic MTs. Scale bar 50 μ m and 20 μ m in the insets.

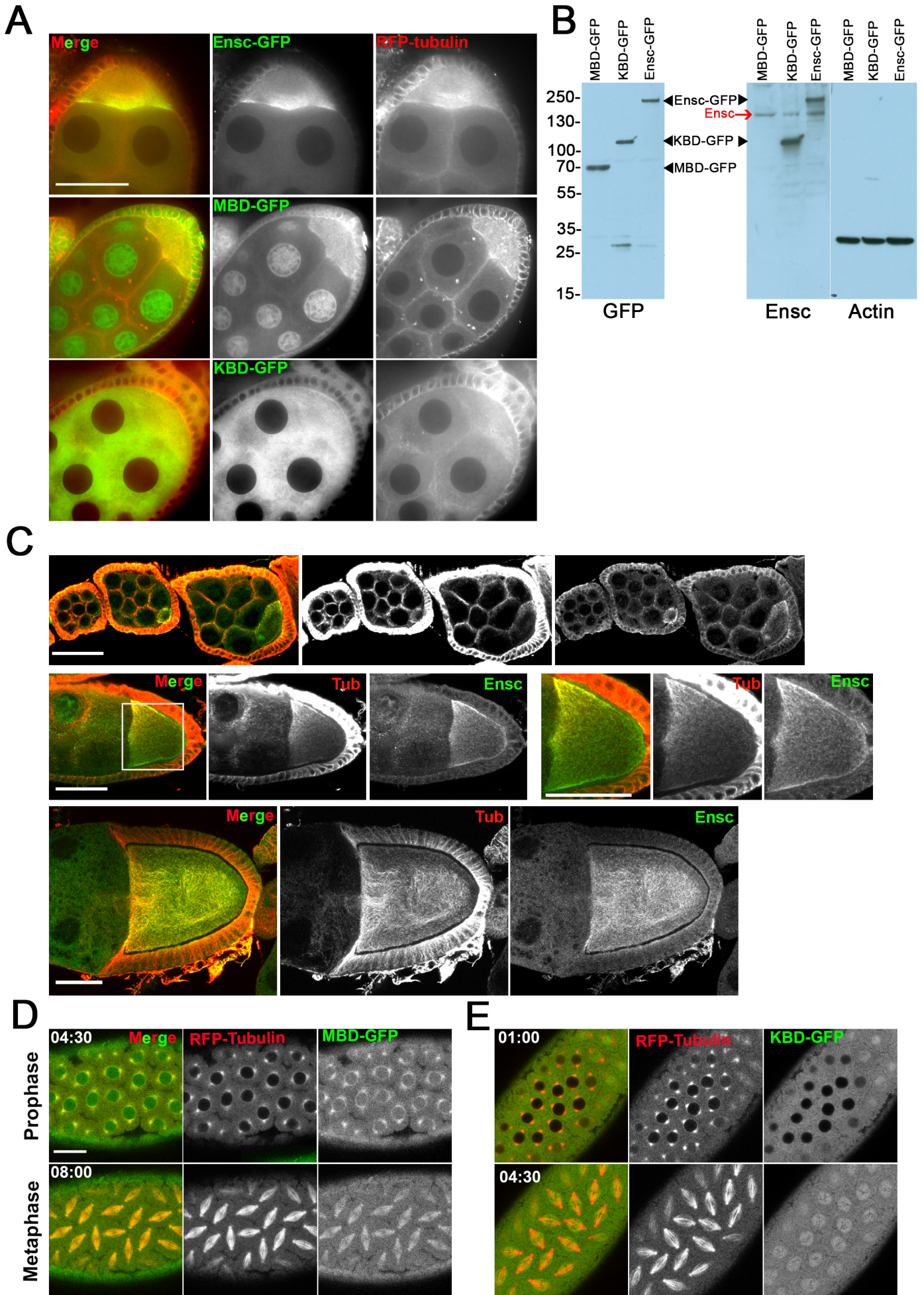


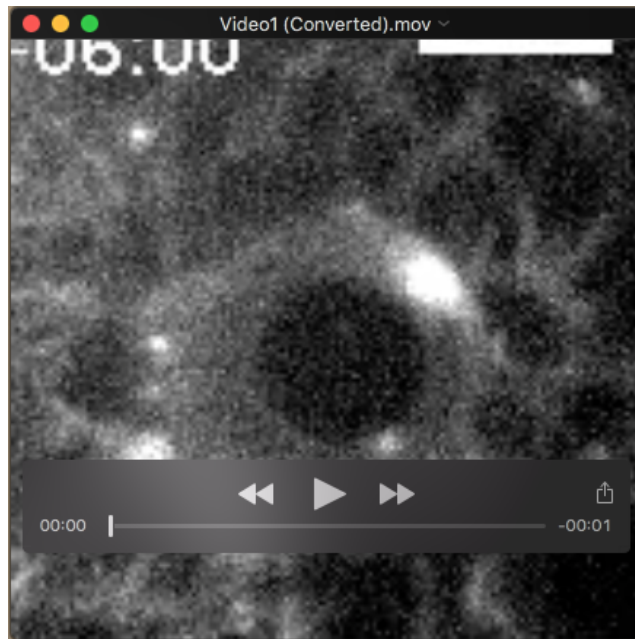
Figure S4. Localization of Endogenous Ensconsin, Ensc-GFP, KBD-GFP, and MBD-GFP variants in oocytes and in live embryos.

A) Live localization of Ensc-GFP (top), MBD-GFP (middle) and KBD-GFP (bottom) in live early oocytes expressing RFP-tubulin (Red in the merge channel), in a wild type background. Ensc-GFP and MBD-GFP are present on the MT network of the egg chamber and of the epithelial cells. KBD-GFP does not localize on the MT network. Scale bar: 50 μ m.

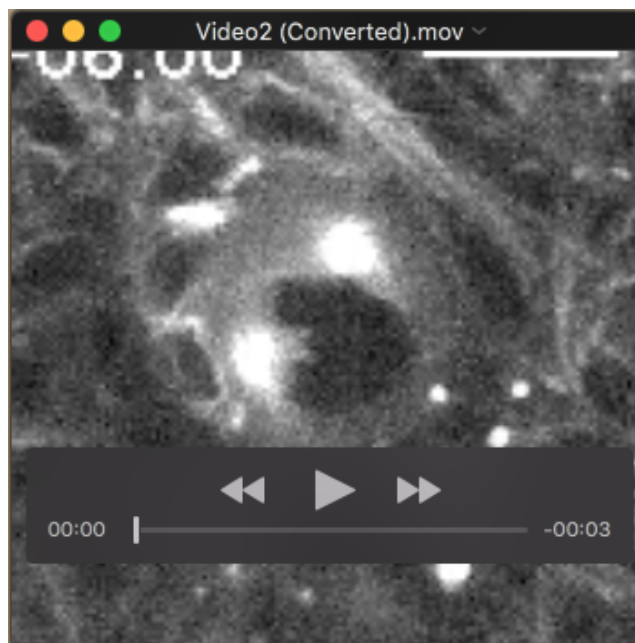
B) Western Blot showing the expression of MBD-GFP, KBD-GFP and Ensc-GFP in ovary extracts from wild type flies. The membrane was probed with anti-GFP antibodies and the three GFP-tagged variants are expressed at similar levels (left). The same membrane was stripped and probed with anti-Ensconsin antibodies raised against the KBD (middle panel). The MBD is not detected. The red arrow indicates the endogenous Ensconsin. The membrane was stripped and probed with anti-actin antibodies (right) as a loading control.

C) Wild type oocytes were permeabilized for 1 h to remove cytoplasmic protein pools (see Methods). They were then fixed and immuno-labelled with an anti-tubulin antibody (red on the left, monochrome elsewhere) and an anti-Ensconsin affinity-purified antibody (green in the left panels, monochrome elsewhere). Scale bars: 50 μ m. Note that Ensconsin is first detected in the egg chamber during early stages (top). At later stages, it co-localizes with the polarised MT network (middle panels). The right panels show an enlarged view of the MT cytoskeleton of the corresponding oocyte. During stage 10B, Ensconsin also co-localizes with the MT network involved in ooplasmic streaming (bottom panels).

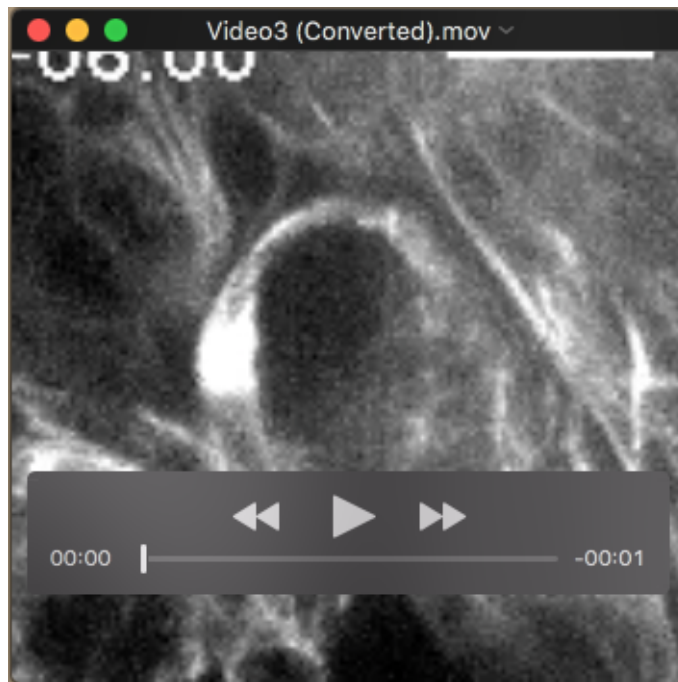
D) Selected images of a wild type embryo-expressing MBD-GFP as it divides during interphase (at 4:30, left) and during metaphase (8:00, right). E) Selected images of a wild type dividing embryo-expressing KBD-GFP, shown during prophase (1:00, left) and metaphase (4:30, right). The GFP-tagged proteins are green and RFP-tubulin is red in the merge pictures, and they are both monochrome in the other panels. Scale bars: 20 μ m. Time is indicated as min:sec. MBD-GFP co-localizes with MTs during mitosis and interphase, but KBD-GFP does not.



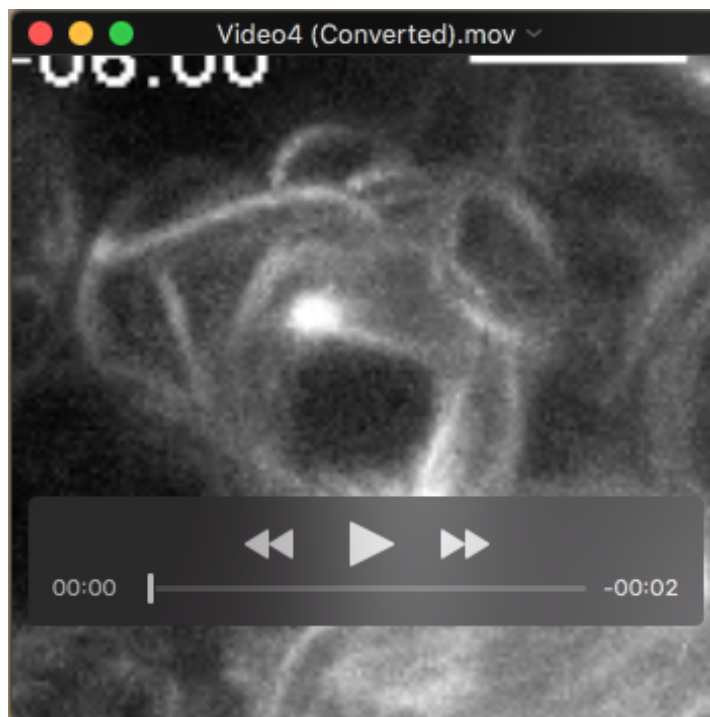
Movie 1. Control dividing NB expressing RFP-tubulin. Scale bar: 10 μ m. Time is min:sec.



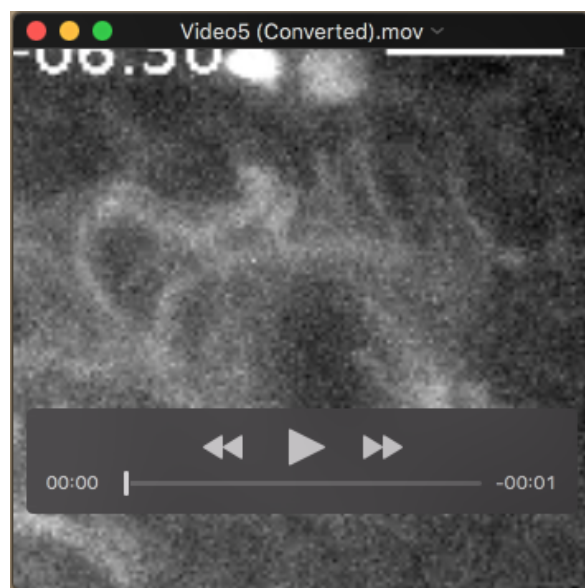
Movie 2. *khc²⁷/khc⁶³* mutant NB expressing RFP-tubulin. Scale bar: 10 μ m. Time is min:sec.



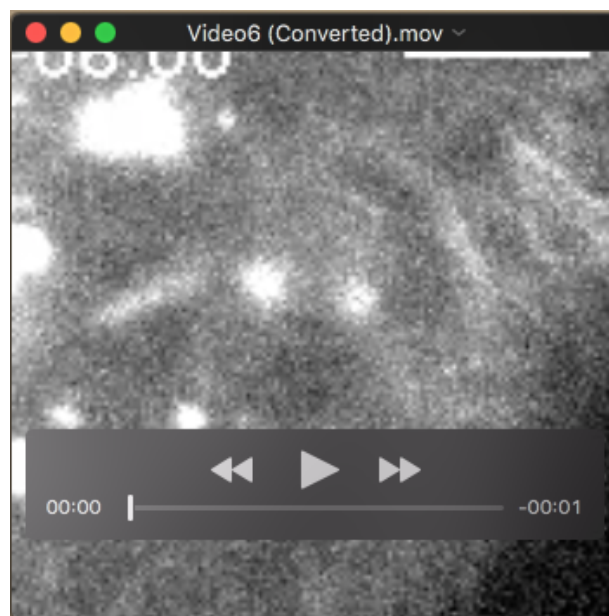
Movie 3. Dividing NB overexpressing Ensc-venus. Scale bar: 10 μ m. Time is min:sec.



Movie 4. *khc²⁷/khc⁶³* mutant neuroblast overexpressing Ensc-Venus during cell division. Scale bar: 10 μ m. Time is min:sec. Scale bar: 10 μ m. Time is min:sec. See the rescue of the centrosome separation defect.



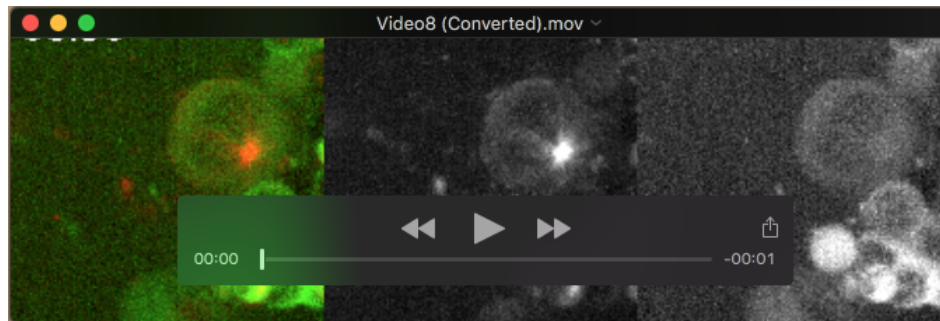
Movie 5. Control dividing NB expressing RFP-tubulin. Scale bar: 10 μ m. Time is min:sec.



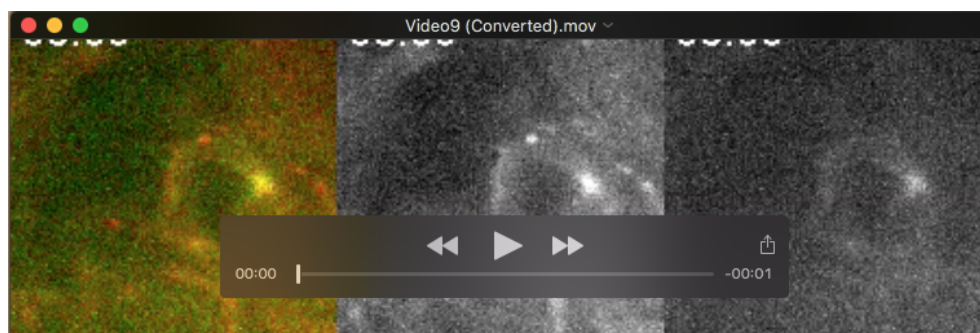
Movie 6. *ensc* mutant neuroblast expressing RFP-tubulin. See the centrosome separation defect. Scale bar: 10 μ m. Time is min:sec.



Movie 7. *ensc* mutant NB expressing RFP-tubulin (red in the merge panel and monochrome in the middle panel) and MBD-GFP (Green in the middle panel, and monochrome in the right panel). There is no rescue of the interphase centrosome separation defect. Scale bar: 10 μ m. Time is min:sec.



Movie 8. Squashed *ensc* mutant NB expressing RFP-tubulin (red in the merge panel and monochrome in the middle panel) and KBD-GFP (green in the merge panel, and monochrome in the right panel). The interphase centrosome separation defect is restored. Scale bar: 10 μ m. Time is min:sec.



Movie 9. *ensc* mutant NB expressing RFP-tubulin (red in the merge panel and monochrome in the middle panel) and full length Ensc-GFP (green in the merge panel, and monochrome in the right panel). Interphase centrosome separation is restored. Scale bar: 10 μ m. Time is min:sec.